Project no. **NMP4-CT-2003-505282**

Project acronym: **BMR**

Project title: **"Ballistic magnetoresistance in thin film nanocontacts"**

Instrument: **STREP**

Thematic Priority: **NMP**

Publishable BMR final Report

Section 1 – Project objectives and major achievement during the reporting period

Section 2 – Present state-of-the art of BMR research in the world

Section 3 – Conclusions

Section 4 – Plan for using and disseminating the knowledge

Period covered: from **1 March 2004** to 3**1 Agust 2007** Date of preparation: 15 October 2007

Start date of project: **1 March 2004** Duration: **42 months**

Project coordinator name: **Professor Genhua Pan**

Project coordinator organisation name: **CRIST, University of Plymouth**

Section 1 – Project objectives and major achievements

The BMR project aims to explore the spin dependent ballistic-electronic transport in thin film nanoconstrictions. The project idea was inspired by the high profile publications in Ballisticc magneto resistance (BMR) in nanowire contacts at the time. The BMR consortium consists of European leading experimentalists (CSIC) in ballistic magnetoresistance (BMR) of wire nanocontacts, leading BMR theorists (KSU), laboratories with the state-of-the-art nanofabrication techniques (CCLRC) and magnetotransport thin films and devices (Plymouth), and leading researchers in spin injection and spin transport studies (IAP), aiming to integrate the complementary knowledge, infrastructure and expertise for the exploration of the spin dependent ballistic transport properties in thin film nanocontacts.

The overall objective of the project is to achieve the development of leading edge nanofabrication techniques (photolithography, e-beam lithography, nanoimprinting and FIB), to employ these techniques in combination with state-of-the-art thin film deposition for the fabrication of thin film nanoconstrictions, and to explore the ballistic magnetoresistance and ballistic spin transport both experimentally and theoretically by carrying out a systematic study of spin transport in these nanocontacts coupled with theoretical analysis.

The major achievements of the project are outlined as follows.

1, Development of e-beam nanofabrication and nanoimprinting techniques

In the duration of the BMR project, we have achieved significant progress in the development of science and nanotechnology including electron beam lithography (EBL), nanoimprint lithography (NIL), reactive ion etch (RIE), lift off process, and nanofabrication techniques for nanostructures and devices.

- **A novel LOR/PMMA bilayer resist technique was developed for high resolution lift off process in electron beam lithography**

The significance of this process is that it has solved the problem related to the reliability of lift-off process. This technique has attracted worldwide attention and has been employed for the fabrication of CIP nanoconstrictions down to 20 nm.

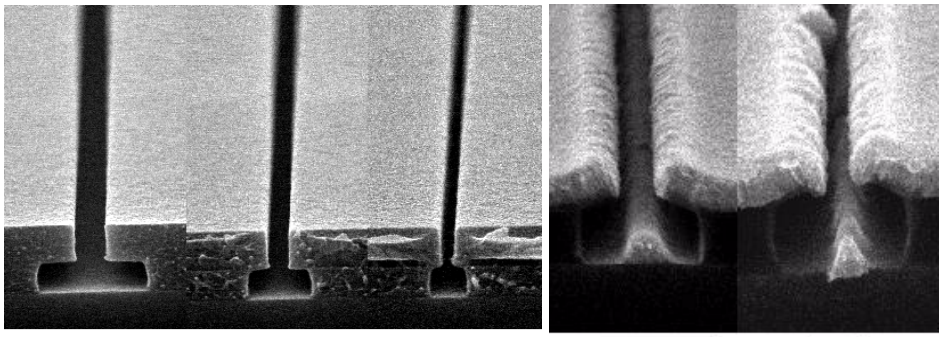

- **World's shortest T gates using the PMMA/LOR/UVIII process was patterned successfully by a two step EBL technique**

This work first introduced a two step electron beam lithography concept for the fabrication of ultra short T gates by the state-of-art e-beam writer system (VB6). The key to achieve such a short T gate is that the two step EBL technique successfully avoided the e-beam spread in the top resist layer (UVIII) caused by the forward scattering effect. This new concept turned out to be a great success and many others are making such short T gates using this technique.

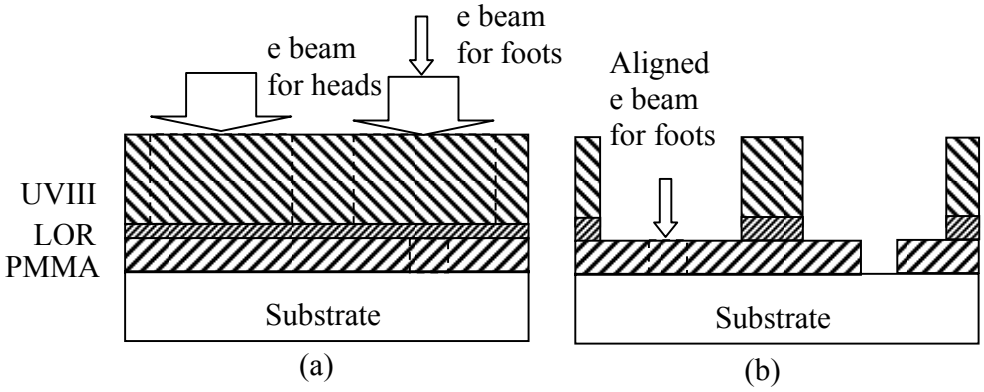

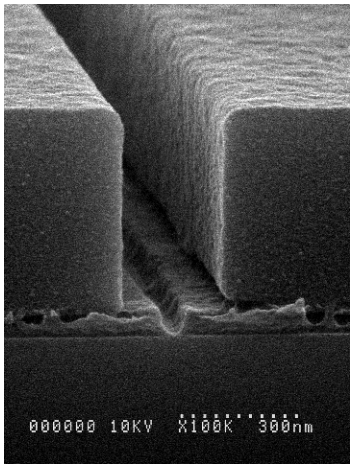

- **Spintronic devices with ultra small nanoconstriction were successfully fabricated**

10-20 nm wide nanoconstrictions in ferromagnetic film have been successfully fabricated with and without an O ring structures, using the developed LOR/PMMA technique for the device configuration of "current in plane" (CIP). This fabrication can now be routinely carried out at RAL of STFC.

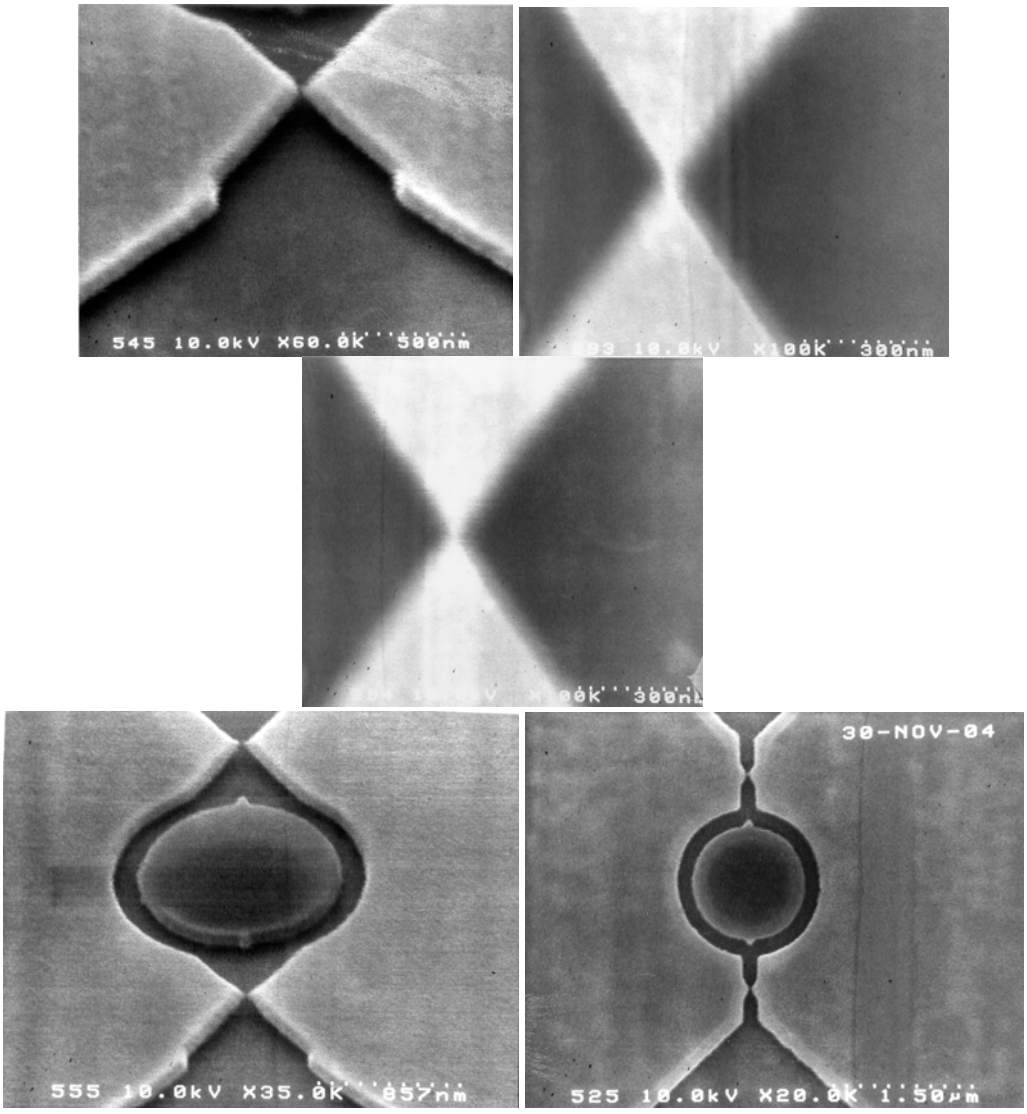

- **Invention of a hot developing process for patterning HSQ resist by EBL**

HSQ resist is a newly commercial resist, which exhibits wide and important applications in semiconductor industry and photonic instruments. However, before this invention (hot developing), the whole community in this field was suffering from a common problem in high resolution and high dense HSQ pattern by EBL. This work introduced the hot developing concept, for the first time in the world, successfully broke through the technique barrier for the patterning of high resolution and high dense structures using

HSQ. Wide applications of the hot developing technique have been observed. Excellent remarks were given by paper reviewers on this publication. (original documents are available). Using this process, ferromagnetic devices with ring structures as well as nanoconstrictions were successfully patterned.

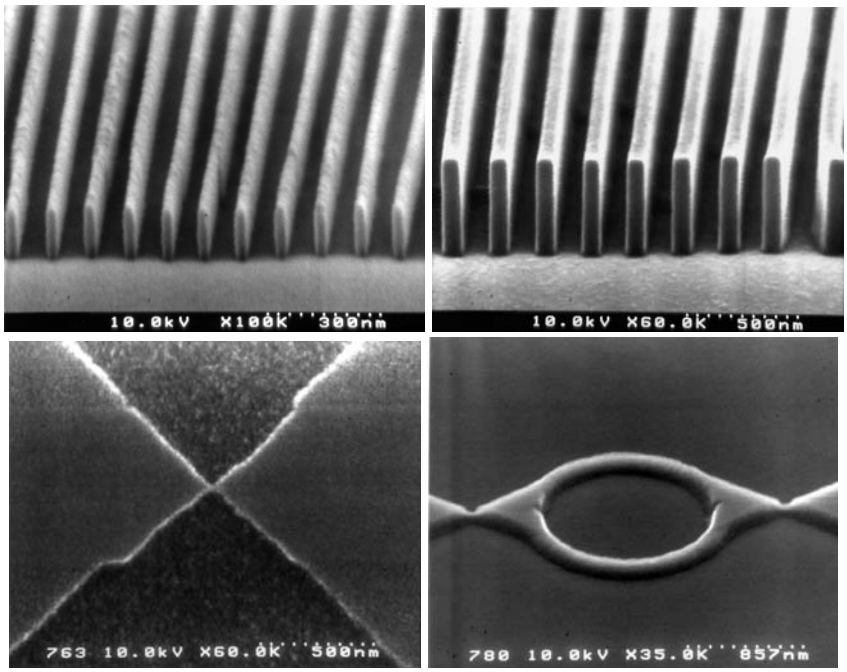

- **Fabrications of nano tips in Si**

Nanofabrication of sharp tips is one of the planned milestone in this project, for the NIL process of nanoconstrictions in vertical configuration. A technique including EBL and RIE process for ultra sharp Si tips with various profiles was developed. The tip radiu is about 3-5 nm. Different profiles of the Si tips can find different applications, for example, AFM tips, imprint tips, nano needles, etc.

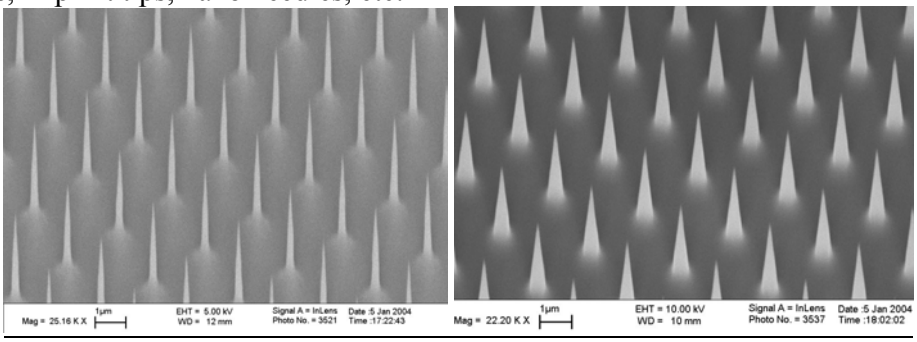

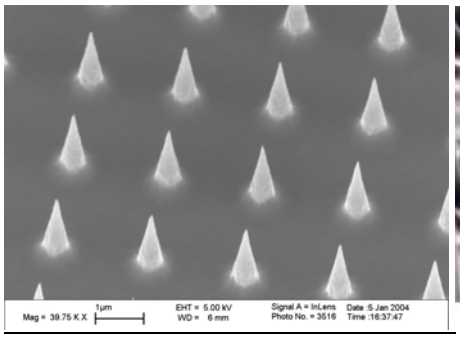

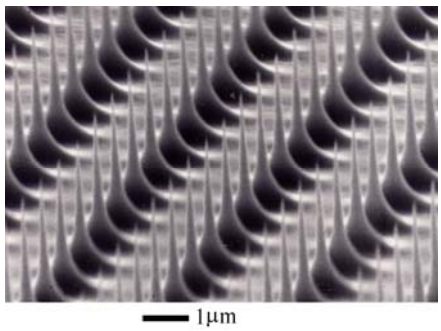

- **Development of nanofabrication technique for NIL templates**

Apart from the above-mentioned Si tips, nanofabrication techniques combining EBL, metal film deposition, lift-off and RIE processes were developed for the fabrications of NIL templates in Si material. Various shape of templates were fabricated: gratings, nano-barcode, nano rulers, chiral shape templates, etc. The smallest feature size is 50 nm and the high aspect ratio was also achieved. The fabricated templates have been provided to Cambridge University, Manchester University, University of Southampton, AML Ltd UK, Fudan University, Institute of Microelectronics, Chinese Academy of Science, He Fei University of Industry, China, etc. Especially the nanobarcode templates sent to the University of Southampton were successfully applied in their EPSRC Basic Technology project, 4G in One Day for the labelling and detection of DNA cells.

This achievement has made RAL of STFC become one of the fewer institutions in the UK, capable of fabricating nanosize templates for NIL and hot embossing technique.

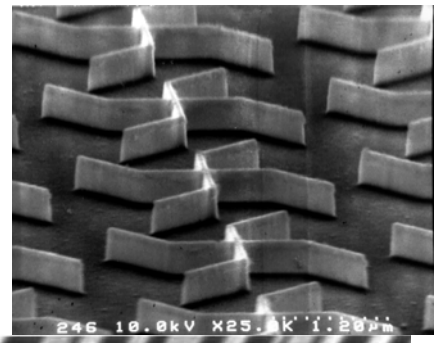

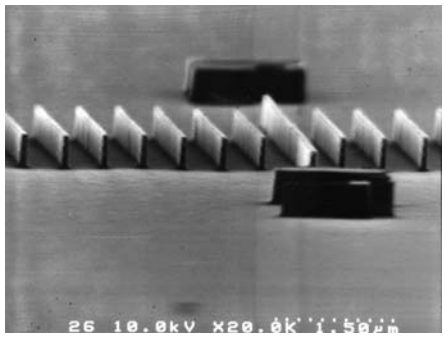

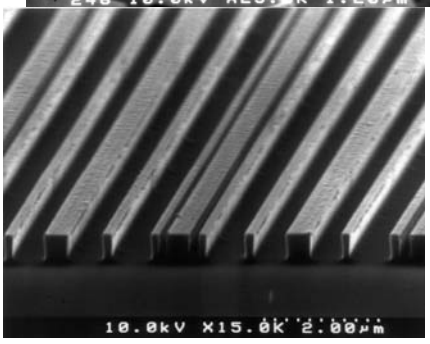

- **Nanofabrication of SiC templates for hot embossing**

In this work, it has been proved that Si template is not hard enough for the NIL. Hard SiC templates were then demanded. In this work, it has been experimentally proved that amorphous SiC film (~1 μm thick) is also hard enough for high pressure NIL and hot embossing. Embossing into metals such as Al has been successfully achieved (see below). The significance of this invention is that manufacturing cost of SiC templates was greatly reduced because SiC single crystal wafers are extremely expensive. A 1 μm thick SiC amorphous film by magnetron sputtering can be used for the hard templates. In this particular, novel RIE process for various templates with various profiles was developed. The profiles include sharp tips, gratings, nanobarcodes and chiral templates.

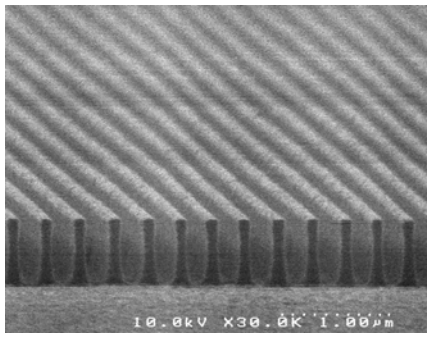

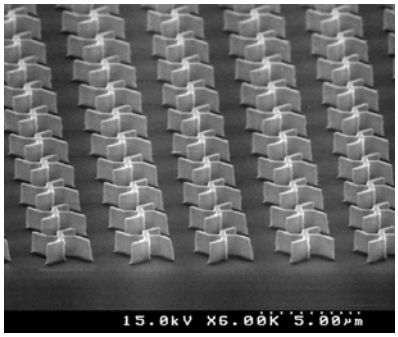

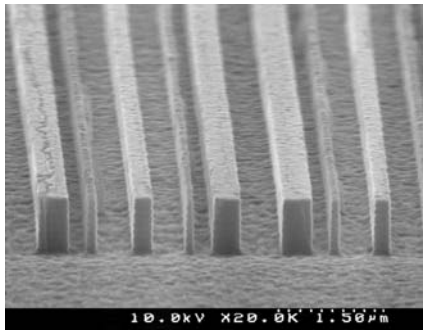

- **Nanofabrications of ultra small pin holes in SiNx dielectrics**

A novel process combining EBL and RIE has been developed for the fabrication of small pin holes in SiNx film. This process was developed for the fabrication of spintronic devices with the configuration of "current perpendicular to plane" (CPP). As small as 30 nm pinholes were achieved and vertical nanoconstrictions in metals have been successfully fabricated. The pin hole size also covers a large range from 30 nm up to hundreds nanometres.

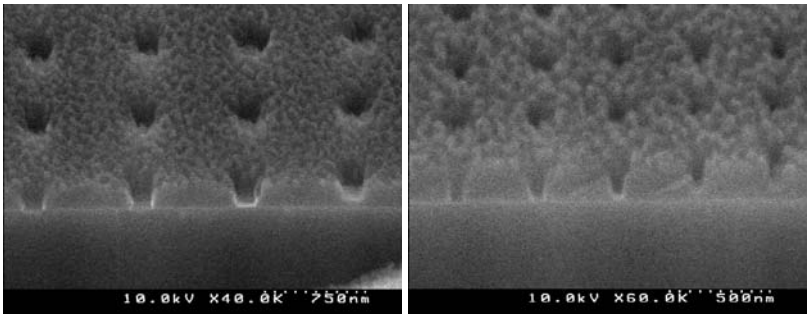

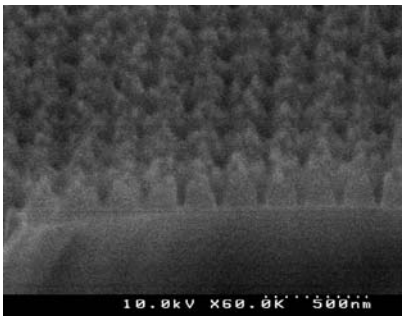

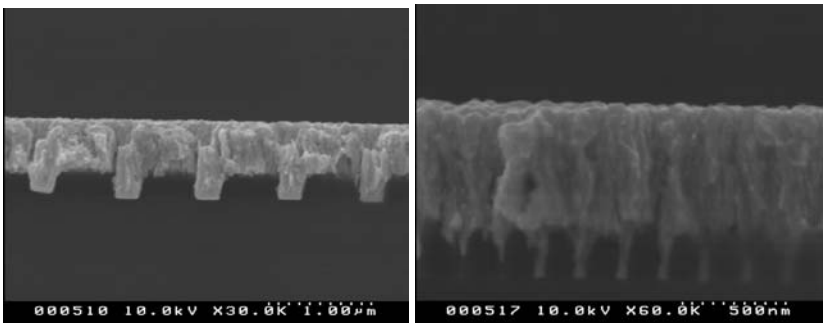

- **A nanoimprint lithography for pinholes in HSQ**

Using the fabricated SiC sharp tips, imprint into HSQ resist was successfully demonstrated. The feature size should go down to 50 nm (but it has not been proved). The NIL tests show extremely uniform imprint structures in large area (1 mm x 1 mm).

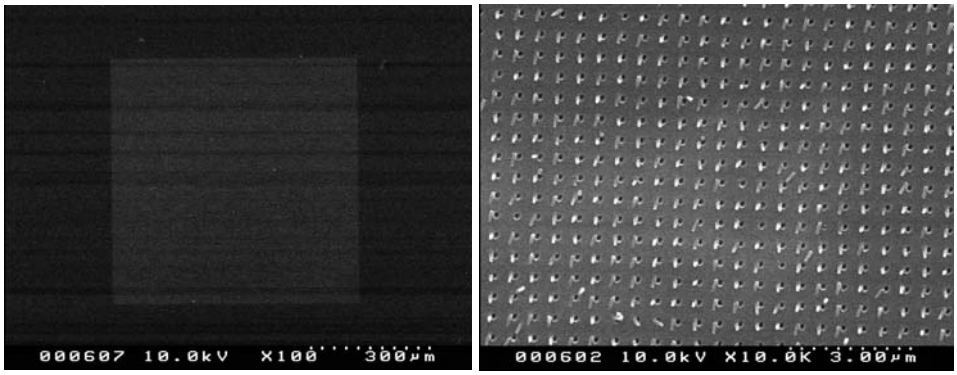

- **A novel nanoimprint lithography using PMMA/HSQ bilayer technique**

To fabricate nanolines in the CIP configuration, a novel process using PMMA/HSQ bilayer technique was developed. The beauty of this technique is that it cleverly used the huge difference in the resistivity to plasma between HSQ and PMMA as well as the ease of imprint into HSQ. This technique has great prospect for the duplication of templates at low cost.

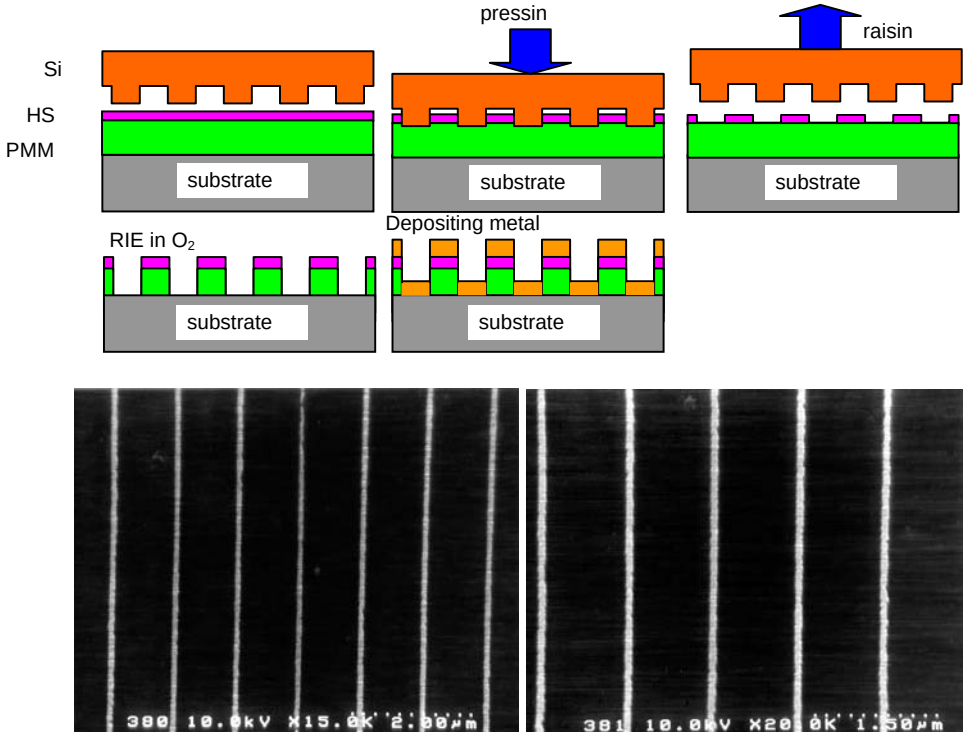

2, Magnetotransport and nanoscale characterisation of constriction devices

- Magnetotransport measurement of CIP nanoconstrictions

By employing the ebeam nanofabrication techniques developed at CCLRC, and the FIB nanofabrication technique developed at IAP, a large number of nanoconstriction samples with a minimum feature at sub 20nm have been prepared. The magnetotransport measurements on this contact showed that a resistance change of 8 ohms was obtainable, however, the magnetoresistance ratio is still very low due to the very high resistance of the contact. During the last 18 months, in addition to the constriction design issues, we have also made the following changes to the samples:

- To reduce the contribution of the long submicron stripe to the total device resistance, we fabricated electrodes with the inner gap width as small as 4/8 μm, which is much narrower than that of previous samples (16 μm).
- Thickness of NiFe films ranging from 7 nm -20 nm.

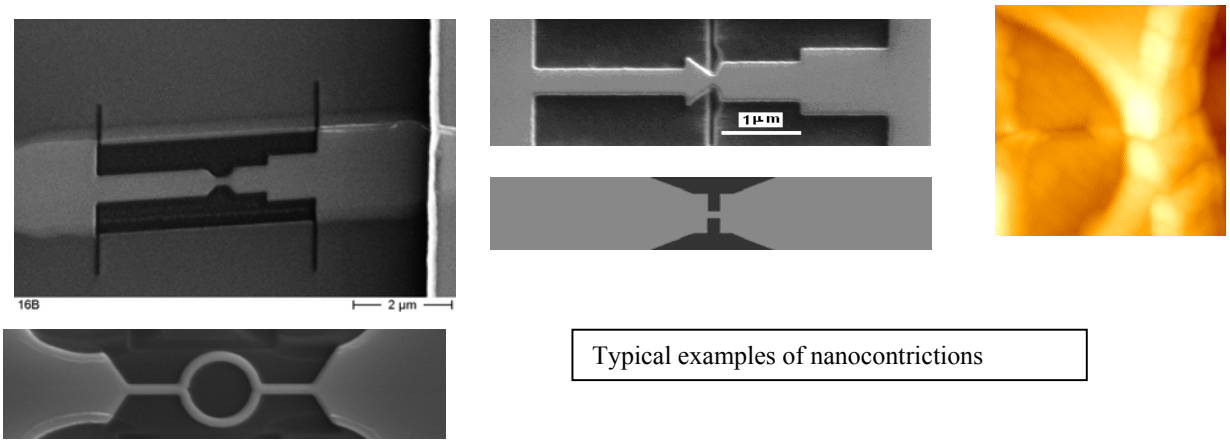

Typical examples of nanocontrictions

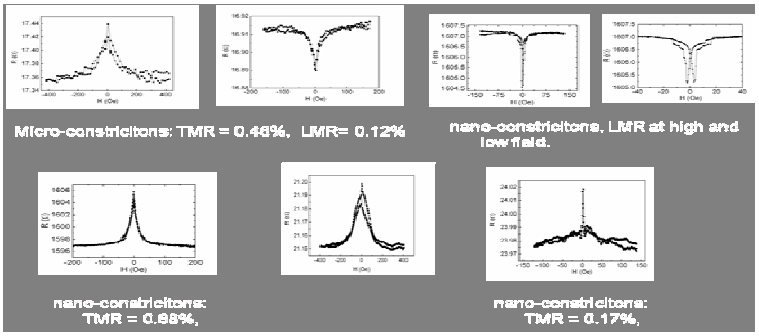

Typical MR curves for various types of nanoconstrictions.

It was concluded from the systematic magneto-transport studies of all these samples that,

- Resistance of nano-constrictions can be reduced by putting electrodes closer together and using thicker NiFe films.
- The amplitude of MR maintains at similar values almost independent of the constriction resistance.
- Values of DR can not be maintained with the reduction of the constriction resistance.
- In all cases, the MR observed has an AMR origin although there are many trivial variations due to the change of film properties, easy axis orientation or other factors.
- No BMR was observed in these constrictions.

The lack of BMR could either be due to the factors that these constrictions were not small enough (outside the ballistic transport regime) or surface oxidation/contaminations may have occurred after the samples were prepared by nanofabrication and opened to the atmosphere during the postal process, or the domain configurations in the constrictions

prevent it from forming the parallel/antiparallel magnetisation configurations inside the constrictions.

- **Spin valve nano-ring samples**

In addition to the single magnetic layered nanoconstrictions, we also carried out the magneto-transport studies of spin valve nanoring constrictions. Spin valve films were pre-patterned into disk shapes at Plymouth, then the samples were sent to Hamburg for FIB nanofabrication. Spin valve nanorings with/without nanoconstrictions and with diameters ranging from 1.6 μm to 500 nm were fabricated and tested. The aim of this part of the work is to employ the domain control characteristics of the nano-ring in an attempt to obtained desired magnetization conficgurations in the nanoconstrictions to obtain possible ballistic transport and ballistic magnetic resistance. Domain configurations of the nanorings were simulated using micromagnetic modeling. The simulation in combination with the MR measurements have revealed that the magnetization reversal processes in the nano-rings was accomplished via either a two-step (from forward onion state to reverse onion state) or a three-step (from forward onion state to vortex state and then reverse onion state) magnetization switching processes depending on nanoring diameters.

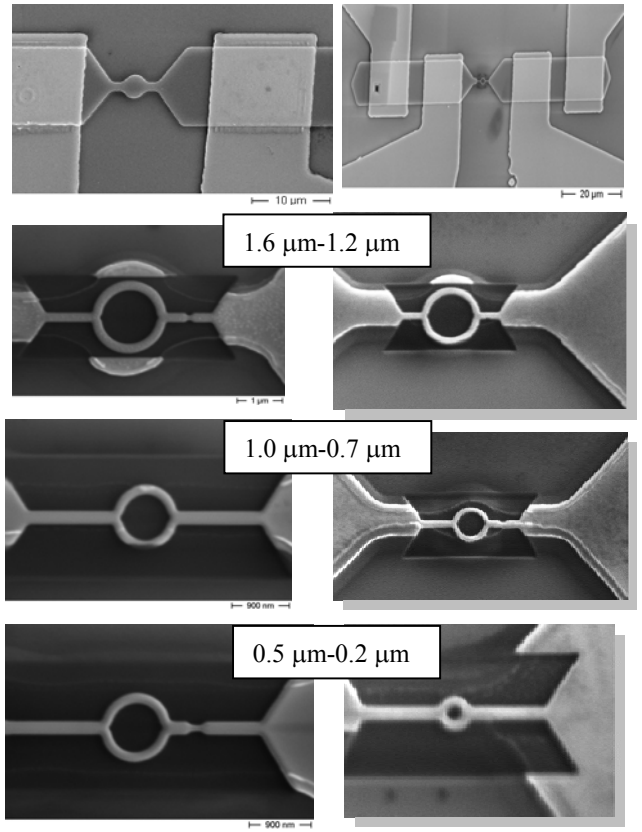

SEM images of spin valve nanorings with different sizes.

Current–assisted magnetization switching and the mechanism of domain control have been studied in a mesoscopic NiFe ring with nanoconstrictions of a wire. It is shown that the applied current has an effect on the switching field and finally on the transition process (single and double switching processes) due to the spin torque effect. For the applied field direction perpendicular to the wire, an enhancement in magnetoresistance ~ 0.12% is

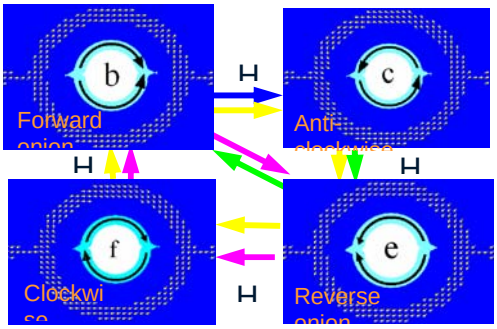

Magnetic reversal processes in the ring (Yellow line for low current, red line for high positive current, green line for high negative current).

obtained at a low applied current as shown in Fig 3, which is due to the domain wall magnetoresistance trapped at nanoconstrictions.

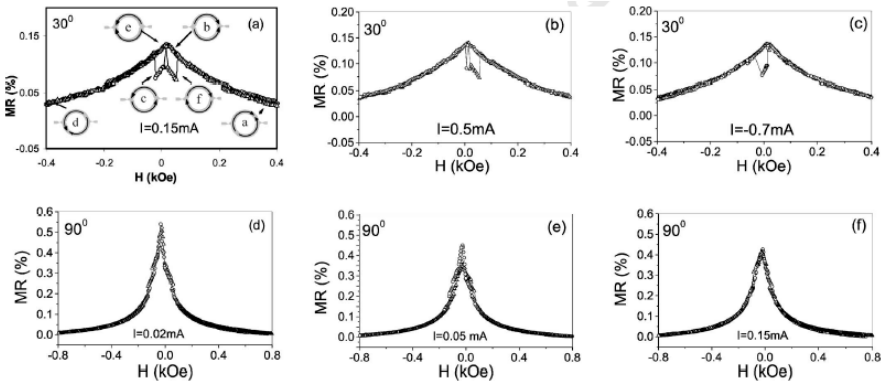

The MR curves for a variety of currents at the different field angles.

Also current-induced domain wall displacement has been studied at CRIST at the nanoconstrictions in both a synthetic spin valve stripe and a pseudo-spin-valve one. It is shown that the critical current density to move the trapped domain wall is typical of the order of 10^7 A/cm^2. Our experimental results demonstrate the feasible manipulation of the domain wall at the nanoconstrictions with the injection of a dc current.

- CPP nanoconstrictions made through SiN membranes

This is based on a novel idea proposed by the Hamburg group. Commercial Si wafers (3x3 and 5x5 in size) with a window of 100 μm in the middle and coated SiN membranes (as shown in Fig 9) were used as the substrate for the CPP nanoconstrictions. FIB milling was employed to mill a nano-pinhole through the SiN membrane. NiFe films were deposited through the hole from one side of the wafer, and CoFe/IrMn films deposited from the other side. In order to achieve the deposition fr4om both sides, the wafers have to be taken out of the vacuum chamber and re-loaded after the deposition of the first side. MR measurement was carried out with 4 point probe method using silver paint to make the necessary connections. A special mask was made to shield the edges of the wafer from deposition of metallic films so that there was no shunting current during measurement. We have carried out this experiment on wafers with two types of SiN membrane thicknesses of 100nm and 30 nm, respectively.

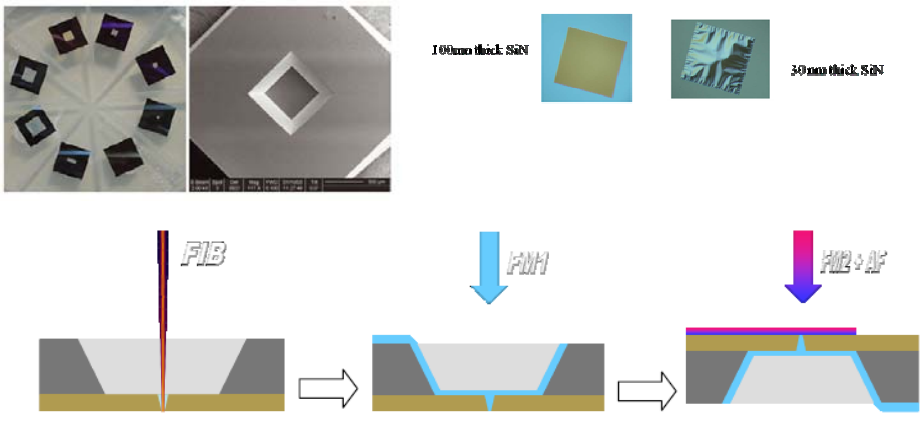

Fig.9, CPP nanoconstrictions on SiN wafers.

For samples with membrane thickness of 100 nm, it was found that the devices were non-conducting. The most likely reason is that aspect ratio of the pinholes are too large and the pinholes are too deep for the films to be deposited through them continuously. However, due to the very small sizes of these pinholes, it was not possible to visually checking the quality of the films deposited through the pinholes.

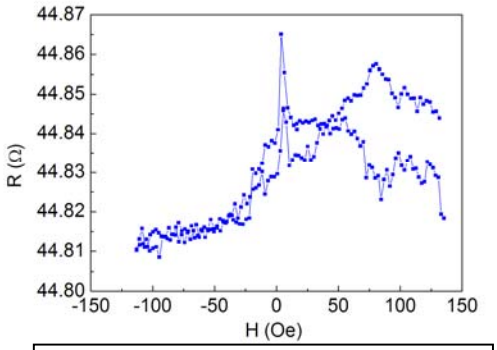

Fig.10, A typical MR curve of CPP nanoconstrictions on SiN membranes.

The samples with membrane thickness of 30 nm were conducting. Fig. 10 shows one of the typical MR curves measured for these nanoconstrictions with layer structure of NiFe 30nm/Ta 4nm on one side and CoFe 6nm/IrMn 15nm/Ta 4nm/Cu 30nm/Ta 5nm on the other. The samples were deposited A number of wafers with different FIB milling conditions were processed. Multilayer films were deposited using different target/substrate separations to optimize the gap filling effect. However, no significant difference was made to the magneto-transport properties of the devices. All the measured MR curves indicated their AMR origin.

In order to clarify the question marks on the quality of the interfaces, we carried out the following experiment:

1. A conventional spin valve stack was deposited following the identical deposition and wafer re-loading sequence. i.e., after the deposition of the first two layers Ta/NiFe, the wafer was taken out of the chamber and reloaded, and then more layers in the sequence Cu/CoFe/IrMn/Ta were deposited after the surface of the first NiFe layer was sputter-cleaned. The CIP MR curve of such a sample is shown in Fig. 11(a).
2. The same layer stacks were repeated on the SiN membrane wafers but deposited through the pinholes. i.e., the Ta/NiFe layers were first deposited on one side of the wafer, the wafer was taken out of the chamber, turned upside down and reloaded, followed by the deposition of the Cu/CoFe/IrMn/Ta layers after the sputter cleaning of the wafer surface. A typical measured CPP MR of the samples was shown in Fig.11(b).

We would expect a CPP spin valve GMR curve from this sample if the interfaces of the layers deposited through the nanopinholes were similar to the sample in Fig.11(a). However, this was not achieved. The MR curve in Fig.11(b) has its AMR origin only. This experiment has shown that it is not an easy task to form the layer stacks inside the nanopinholes in the form as we would hope for. It presents the difficulties in realizing

CPP nanoconstrictions in the SiN membrane samples.

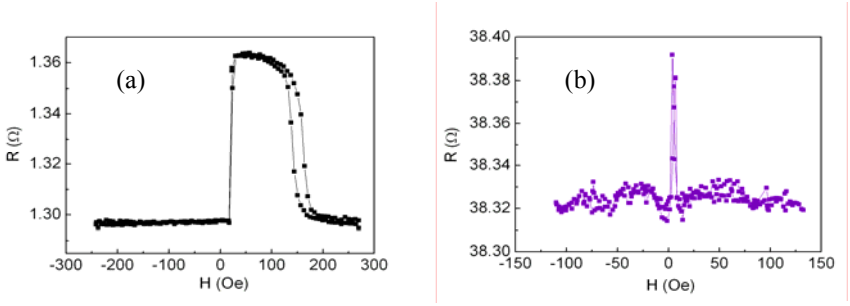

Fig. 11, CIP MR curve of a spin valve stack (a); CPP MR curve of a similar stack deposited through nanoconstrictions made in the SiN membrane

3, FIB nanofabrication and in-situ magneto-transport measurement of thin film nanoconstrictions

We have started with the fabrication of nanoconstrictions in CIP structures delivered by CRIST. Such a nanoconstriction made in a e-beam pre-patterned permalloy is shown below.

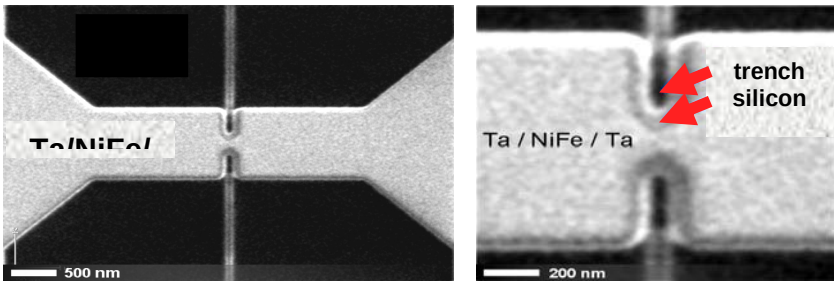

FIB fabricated nanoconstriction. The constriction is made by milling a line from top and bottom into the pre-patterned pad. On the right-hand side a magnified image reveals the different milling cycles. At first the broader structure is milled which removes the ferromagnetic material. After that the sharp lines are milled to prevent any by-pass resistance.

The transport measurements revealed that domain walls are not pinned in such structures. The conventional AMR effect has been observed. The structures were changed accordingly. The e-beam structures as well as the shape around the constriction, which is structured by FIB, was altered. With such new structures we found evidence for the magnetoresistance due to magnetic microstructures within the constrictions.

During the first investigations it turned out that a major problem with the small constriction is the instability against contamination and oxidation. Frequently it was found that material on the constriction caused the destruction of the electrodes when current was driven through the thin film structure. Secondly, the constriction became instable against oxidation the smaller the structure was. The partner discussed that problem on the 30 months meeting and decided

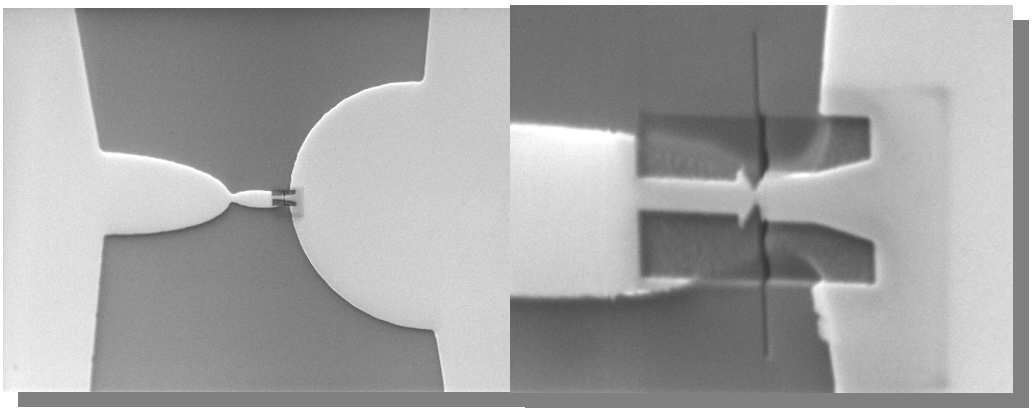

The modified structure for domain wall injection and pinning. The picture on the left-hand side gives an overview of the structure made by e-beam lithography. The magnification on the right-hand side reveals the manipulation on the structure performed by FIB.

to change the strategy. The main improvement was expected from switching to an all UHV-experiment, which means that the structures are fabricated and the transport investigations are performed in-situ. This measure should prevent contamination and oxidation of the constriction. Additionally it allows for a parallel production of a large set of different nanoconstrictions on one and the same thin film sample. The idea had been to implement into the FIB system a micromanipulator which allows to measure the resistance of a single nanoconstriction.

The constriction which is created by FIB milling connects an insulated nanostructure and the rest of the film. Via the micromanipulator the insulated part is connected while the film is grounded and a current can be driven to ground through the constriction.

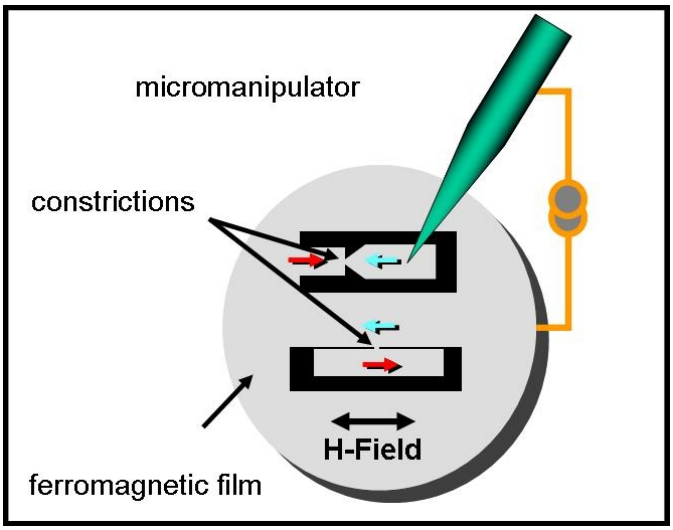

Sketch of the set up of in-situ magnetotransport measurement. The thin film ferromagnet is deposited on an

insulating substrate. Nanostructures are created in the film by FIB. Every point of the nanostructure can be connected by means of the micromanipulator. The current flows between micromanipulator tip and ground.

The final successful realization of the new tool can be seen in the Figure below. The photograph gives the view into the FIB chamber. The thin film sample is in between two pole pieces of a self-made electromagnet and can be structure by the FIB (from the top). A thin W wire is welded to the top most end of the micromanipulator which allows to make the contact to nanostructures (see inset). The realization and assembling of the device took some time which blocked work with the FIB.

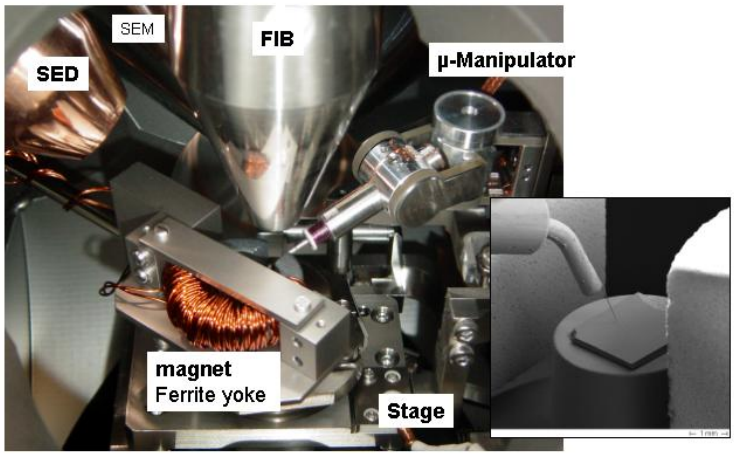

View into the FIB system with yoke and micromanipulator. The inset shows the thin film sample between the pole pieces and the end of the micromanipulator with the attached W-wire.

The results justify the efforts. We have very successfully investigate the size dependent resistance and magnetoresistance of FIB fabricated constrictions utilizing this new tool. As nanostructures that show stable domain pattern we have selected ellipses which are known to exhibit a vortex structure for the chosen dimensions in permalloy. This was cross checked and proven by SEMPA (Scanning Electron Microscopy with Polarization Analysis) and MFM (Magnetic Force Microscopy). The domain pattern in such ellipses is shown in the Figure blow.

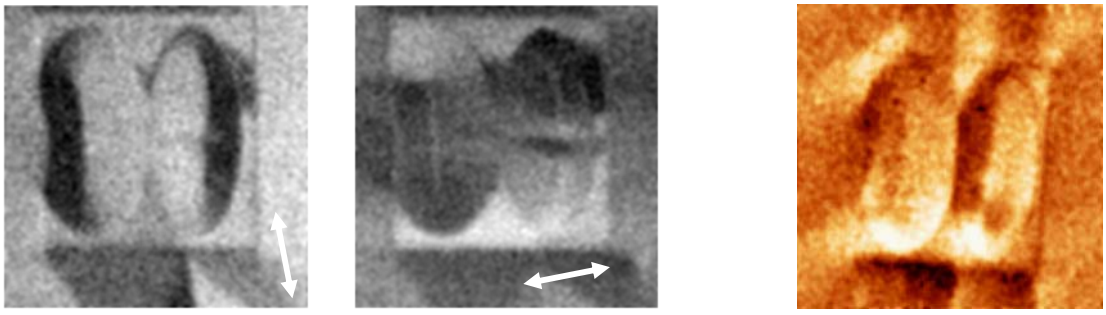

Domain structure of ellipses. The two SEMPA images on the left-hand side display the polarization distribution in two perpendicular polarization (magnetization) components. The arrows indicate the polarization sensitive axes. On the right-hand side the MFM image of the same structure is shown (image sizes 15 x 15 µm²).

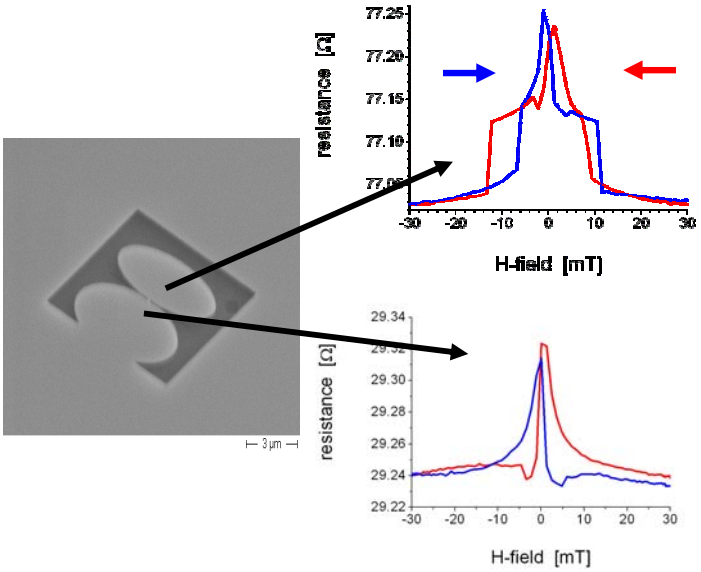

Magnetotransport measurements across an ~ 80nm constriction. The constriction is located between the two ellipses. The two measurements were obtained when the micromanipulator was positioned on the smaller and the larger ellipse respectively. The color indicate the sweep sequence of the field oriented along the long axis of the ellipse. The constriction causes a steep increase/decrease of the resistance between 10 and 20 mT.

The two ellipses fabricated in a Py film have different sizes to achieve different magnetization behavior, which means that the magnetic microstructure is altered within external fields at different field strength. The smaller ellipse is connected to the larger one via the constriction that is intended to be investigated. The larger ellipse has a wide connection to the whole film. In a series of experiments we have investigated the magnetoresistance as a function of constriction width. One example of the magnetoresistance as a function of magnetic field is plotted on the right-hand side of Fig. 6. The width of the constriction is ~ 80 nm. At first it is evident that when contacting the small ellipse the resistance is more than double that obtained when connecting the larger ellipse. As the tip is located as close as possible before and behind the constriction we can appoint the difference unambiguously to the resistance of the constriction. The contribution of the constriction is given by a step like increase of the resistance at fields far above or below zero field. The resistance drop is more pronounced than the raise. That structure is due to a domain wall that is inserted into the constriction when lowering the field strength as the vortex structures evolve in the ellipses. The resistance increase is due to a 180° wall that separates two vortex structures with opposite sense of rotation. This is to our knowledge the first measurement that shows unambiguously the separation of domain wall resistance. A paper about this highly interesting results is under preparation.

The whole set of experimental data are put together in Fig. 7 which shows the constriction resistance as function of the width (blue rectangles). As one would expect we find an increase of the resistance with decreasing width. The maximum resistance change (red dots) increases go from 200 nm to smaller nominal constriction widths. The increase is most likely due to the change of domain wall structure as the latter is dependent on the constriction dimensions.

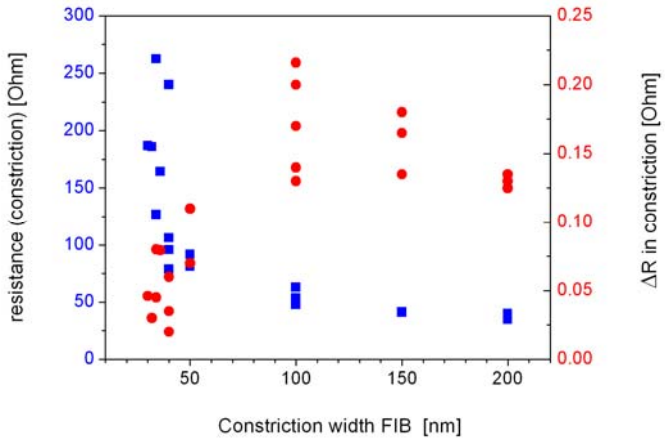

Resistance and maximum resistance change in constrictions as function of nominal constriction width. Due to the Gaussian distribution of the ions in the beam the constriction is actually smaller than the number which are given here. The blue rectangles give the resistance while the red dot give the maximum resistance change of the constriction in magnetic field.

A further decrease of constriction dimension let the maximum resistance change drop to small values. The same is found also for the magnetoresistance of the constrictions (Fig. 8) although the increase (between 200 and 100 nm) is difficult to see due to small resistance change here. At the moment we cannot explain all the details of that behavior. Micromagnetic simulations of the domain wall structure and theoretical treatment of its resistance have to be performed to identify the different effects behind our findings.

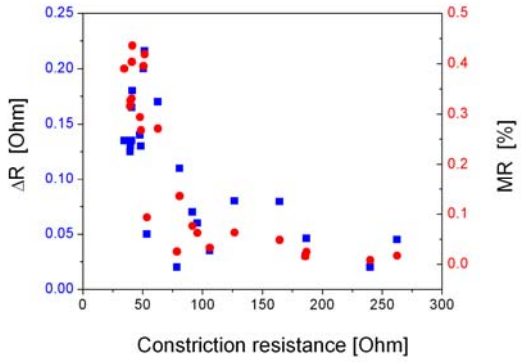

Magnetoresistance and resistance change of constrictions in magnetic fields. The nominal constriction width can be appointed to the resistance values using the results plotted in the previous figure.

In particular the strong drop for the smallest structures has to be explained first. The magnetoresistance curves for the very small constrictions (Fig. below) do not show any features that could be appointed to the influence of the reduced dimensions in the constriction. The measurement exhibits the normal AMR characteristic of a film with high resistance.

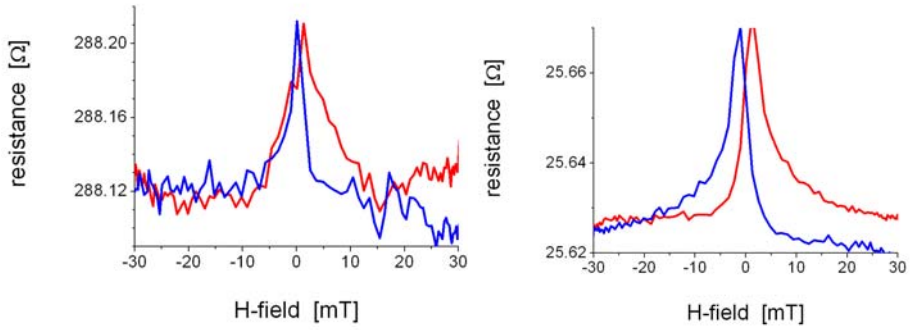

Magnetotransport measurements across a sub-20nm constriction. The measurement across the constriction is displayed on the left-hand side. The two measurements show the same characteristic. No traces of additional structures due to the cvonstriction can be identified.

One possible explanation is that in the smallest constriction the remaining material is no longer ferromagnetic due to destruction caused by the ions. The second possibility is that the domain wall structure has changed because the width to length ration of the constriction has reversed in the smallest constrictions.

In summary we can conclude that the in-situ investigation of nanoconstrictions has revealed unexpected new effects. We were able to measure the magneto resistance of a single domain wall for the first time and its evolution as a function of the constriction width. As the constriction width influences the domain wall properties strong variations of the magnetoresistance are found. The further analysis needs a more theoretical modulation.
We do not find any evidence for BMR. The reason for that can be manifold. What is sure is the fact that not only the width of the constriction but also the length of the constriction is important particularly with respect to the magnetic microstructure that does or does not evolve in such a structure. In general one can expect that for small scaled constrictions (with small length) the magnetic microstructure might ignore the existence of the "zero length imperfection" and BMR will not appear.

4, BMR theory

Task 6.1, model for ferro-NC (KSU, CSIC, CRIST)

The influence of the domain wall profile, its dependence on magnetic field, the relaxation of the electron spin on the magnitude of BMR will be investigated for ferro-NC. The influence of spin-asymmetry of scattering on impurities will be analyzed at marginal, but

realistic situation, when one spin-channel has ballistic conductance, whereas the other one is still in diffusive regime. Another portion of the work will be concentrated on studies of non-symmetric nanocontacts made of two different ferromagnets. The conditions to maximize BMR effect will be clarified.

Task 6.2, model for hetero-NC (KSU, IAP)

Nanocontacts made of hetorostructural magnetic materials (ferromagnet/semiconductors, ferromagnet/insulator/ semiconductor, etc.) will be investigated, possible regimes of conduction through the contacts will be considered and expected spin-polarization of the current is estimated. Tunnelling magnetoresistance in point contacts will also be calculated in the framework of the model developed previously by the authors and in conjunction with the new experimental data obtained. The statistics of the tunnelling current distribution and conditions to obtain maximal TMR will be searched on.

The division of the tasks on sub-tasks are as follows:

6.1.1 – the influence of the domain wall profile;
6.1.2 – the relaxation of the electron spin upon transmission through the contact;
6.1.3 – the influence of the spin-asymmetry of the bulk impurity scattering on the magnetoresistance of ferromagnetic nanocontacts;
6.1.4 – magnetoresistance in non-symmetrical nanocontacts made of two different ferromagnets (ferromagnetic heterocontacts);
6.2.1 – the boundary resistance of the interface between two conductors;
6.2.2 – the boundary resistance of the interface between ferromagnetic and non-magnetic metal, implications in the giant magnetoresistance effect;
6.2.3 – magnetoresistance of magnetic tunnelling nanocontacts.

Works performed in this subtasks are as follows:

The **sub-task 6.1.1** was carried out in the direction of studying the domain wall magnetoresistance (MR) of quantum magnetic nanocontacts. The influence of the nanocontacts cross-section shape (from cylindrical to rectangular) and the domain wall profile (from sharp, step-like to the extended, linear one) was investigated [1,2,12,13], and it was found that:

(a) the magnetoresistance crucially depends on the cross-section shape of the nanocontact. In fact, the dependence of MR on the number of open conductance channels (Fig. 1, panels (c) and (d)) has no allowed values at conductances $\sigma^F=3e^2/h$, $\sigma^F=5e^2/h$, *etc*., whereas the measured MR has [N. Garcia *et al*, PRL/1999].

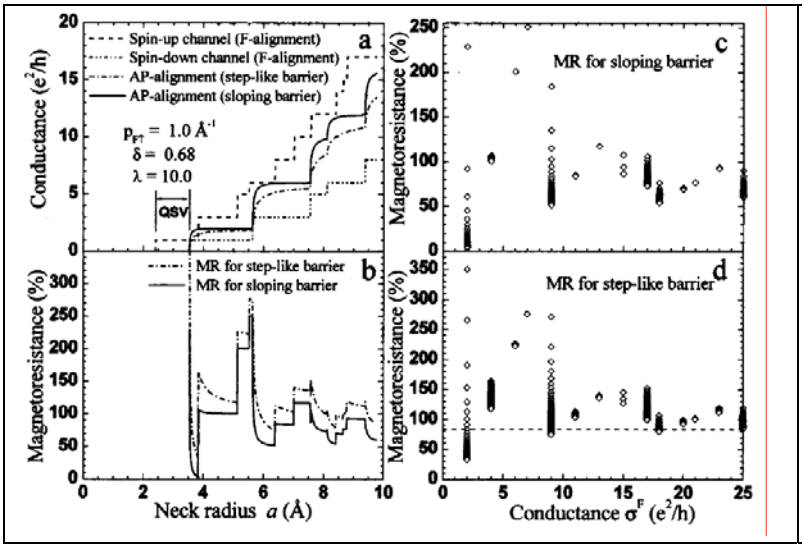

Fig. 1. The dependence of conductance (a) and magnetoresistance (MR) (b) on the radius of the cylindrical cross-section nanocontact. Panels (c) and (d) show dependence of MR on the number of open conductance channels for the ferromagnetic alignment of magnetizations in the electrodes. The maximal MR=582% for the step-like shape of the domain wall at $\sigma^F=2e^2/h$ is not shown.

The possible solution of the discrepancy is the non-circular shape of the nanocontact cross-section which eliminates degeneracy of the geometry in the contact plane, thus allowing the intermediate conductance magnitudes which show magnetoresistance. To demonstrate that this idea works we have made calculation for the rectangular shape of the cross-section and have shown that now magnetoresistance is allowed for every numer of open channel of conductance for the ferromagnetic alignment of magnetization in the electrodes (Fig. 2, panels (c) and (d)).

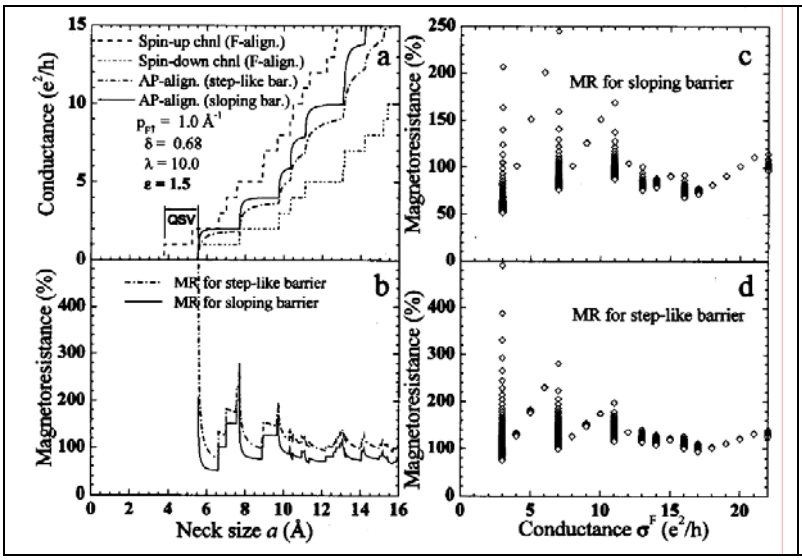

Fig. 2. The same as in Fig. 1 but for the rectangular cross-section of the nanocontact. The maximal MR=758% for the step-like shape of the domain wall and MR=322% for the linear shape of the domain wall at $\sigma^F=3e^2/h$ are not shown.

(b) the magnetoresistance can be calculated with more realistic profile of the magnetization rotation along the nanocontact length: linear [P. Bruno, PRL/1999] instead of the step-like. As a result, the magnetoresistance magnitude decreases, however, not so drastically (panels (c) in Figs. 1 and 2 compared with panels (d)). Thus, the finite domain wall length does not kill the domain wall magnetoresistance effect.

(c) with the rectangular shape of the nanocontact cross-section, and the finite

domain wall thickness we could satisfactorily reproduce the N. Garcia's MR data on a first few of open conductance channels in Ni-Ni and Co-Co nanocontacts (see the representative data for the Ni-Ni nanocontacts in Fig. 3).

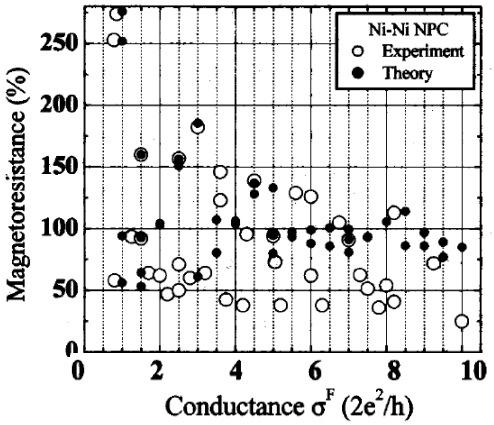

Fig. 3. The experimental data (N. Garcia) and the calculated points for MR in Ni-Ni point nanocontacts.

Within the **sub-task 6.1.2** we investigated the influence of electron-spin relaxation upon transmission through the contact on the magnetoresistance of the quantum magnetic nanocontacts [2,3,14-18]. If conductance of a magnetic nanocontact is quantized, earlier or later the magnetoresistance becomes infinite upon decrease of the contact size (see upturn of MR data in the panels (b) of Fig. 1 and Fig. 2). It is consequence of the conductance quantization, because of which the antiparallel alignment conductance of the nanocontact is zero at the first conductance step for the parallel alignment of magnetizations. Any bypass conduction will limit this unphysical divergence of MR. The most plausible mechanism of the bypass conduction is reversal of the electron spin upon transmission through the nanocontact. We have studied the domain wall tracking by the electron spin as a dominating mechanism of the electron spin reversal. We applied the quantum scattering theory as a basic formalism to calculate the electron-spin reversal time. The key point of the study is the utilization of exact solution of the particle motion in a sloping potential of the geometrically constrained domain wall (Fig. 4) as a zero-order approximation for ballistic transmission through the magnetic domain wall.

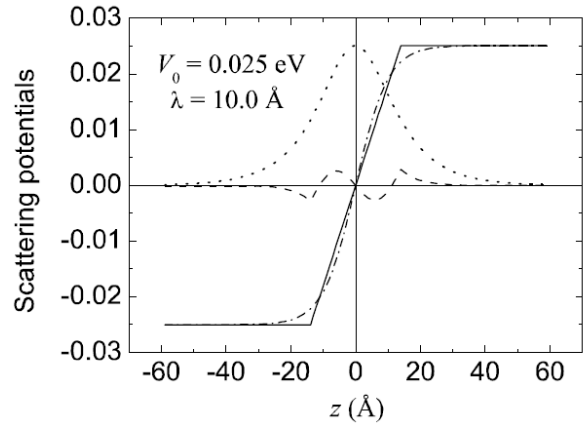

Fig. 4. Scattering potentials: black – Cabrera-Falicov spin-conserving, blue - Cabrera-Falicov spin-flip, red – model sloping potential, green – difference of Cabrera-Falicov spin-conserving and the sloping potentials, considered perturbatively.

Exact Green functions of the quantum scattering problem have been found using wave functions of the exactly solvable problem, and probabilities of ballistic transmission for the conduction electron without tracking the domain wall profile (spin-conserving) and with tracking the domain wall profile (with spin-flip) have been formulated in the perturbation approach. The spin-conserving probability was calculated in the first-order in difference between the sloping shape of the domain wall potential and a realistic shape, for which the Cabrera-Falicov potential has been used. The spin-flip transmission probability has been calculated in the second order on the Cabrera-Falicov spin-reversing potential. Conductance of the ballistic nanocontact is proportional to the above transmission probabilities (see Fig. 5). The inset shows the spin-flip conductance

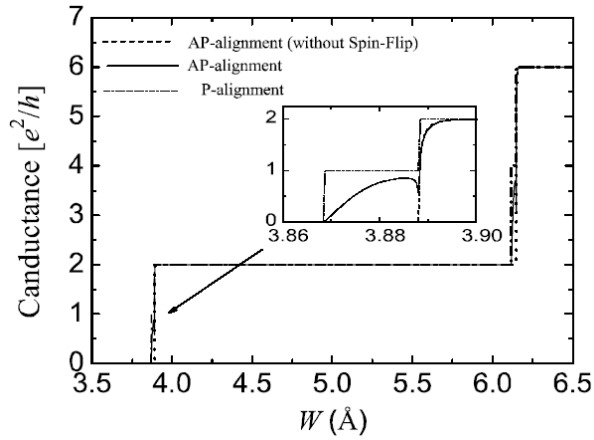

Fig. 5. The conductance as a function of the transverse dimension W in cases; (a) parallel alignments of magnetizations, (b) antiparallel alignments of magnetizations with spin flip scattering, and (c) without spin flip. Here we take the Fermi energy ε_F = 3.0 eV and the contact length λ = 10 Å.

.

inside the first step of conduction at parallel alignment of magnetizations. We have shown for the first time that the spin-flip conductance, which is forbidden without DW profile tracking (or another spin-flip process, spin-orbit interaction, for example), prevents infinite growth of the ballistic magnetoresistance (MR) in the contacts with quantized conductance (Fig. 6, solid lines – compare with the dash ones).

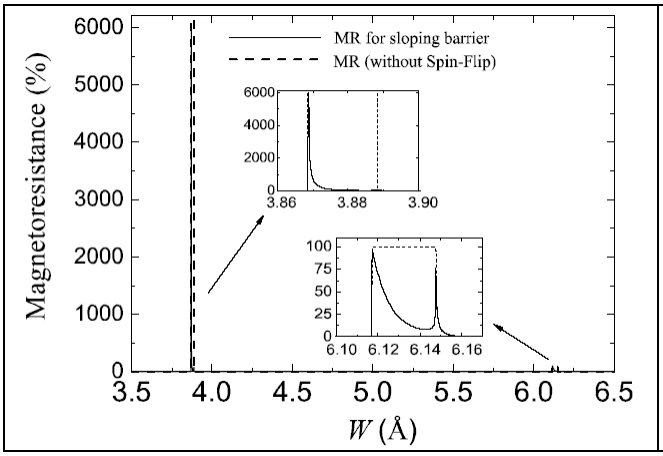

Fig. 6. Domain wall magnetoresistance of the nanocontact as a function of the cross-section size W. The parameters are the same as in Fig. 5. The MR with spin-flip shown by solid lines, without the spin-flip – by dash curves.

.

The approach that we developed here is universal: any other relevant shape of the domain wall and spin-reversing potential can be easily incorporated into the computer program instead of the Cabrera-Falicov ones.

In the **sub-task 6.1.3** the magnetoresistance of the nanocontact between two ferromagnets with non-equivalent spin-asymmetries of the bulk impurity scattering has been investigated [5,19]. The key point here is as follows: small amount of *3d* and *4d* impurities may affect drastically the bulk spin-dependent mean free paths of conduction electrons in ferromagnetic metals [M.B. Stearns, JAP/1977; JMMM/1991]. At the same time, the Fermi momenta and the band widths remain practically unchanged. Then, one has a freedom to vary spin-up and spin-down mean free paths in the electrodes independently in a wide range. As a result, at a certain combination of the spin-dependent mean-free paths (Fig. 7c, and Ref. [6] for further details) there is a hint that MR can decrease much more slowly. As we'll see below, in ferromagnetic heterocontacts this effect is much more pronounced.

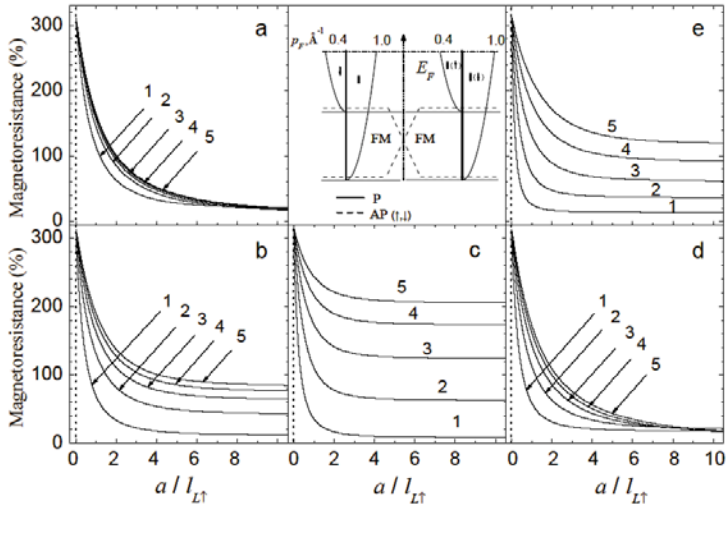

Fig. 7. Magnetoresistance of a ferromagnetic homocontact with different spin-asymmetries of the sides. The spin-polarization parameter $\delta_L = p^L_{F\downarrow}/p^L_{F\uparrow} = 0.4 = \delta_R$, the contact length is 1nm. The central window in the first row represents the conduction-band matching diagram for the contacting ferromagnets. Labels 1 to 5 indicate the spin-asymmetry parameter of the right-hand side ferromagnet as follows: $l_{R\uparrow}/l_{R\downarrow}$=5.0, 2.0, 1.0, 0.5, 0.2. The graphs labeled from (a) to (c) are drawn for the spin-asymmetries $l_{L\downarrow}/l_{L\uparrow}$=5.0, 2.0 and 1.0, respectively, and $l_{L\downarrow}/l_{R\downarrow}$=1.0.

	Graphs (d) and (e) are drawn for $l_{L\downarrow}/l_{L\uparrow}$=5.0 and $l_{L\downarrow}/l_{L\uparrow}$=2.0, respectively, and $l_{L\downarrow}/l_{R\downarrow}$=3.0.

In the **sub-task 6.1.4** the magnetoresistance between two different ferromagnets has been investigated [5,6,7,20] (the case of ferromagnetic **hetercontacts**). We derived quasiclassical expressions for magnetoresistance (MR) of ferromagnetic heterocontacts which are valid for arbitrary spin-polarizations of the conduction band of the electrodes and spin asymmetries of the conduction electron bulk scatterings [5,7]. It is very realistic situation when the spin-up and spin-down mean free paths may differ up to 5-7 times. For example, in permalloy, $l_{L\downarrow} \approx 6$Å, whereas $l_{L\uparrow} \approx 43$Å, so that the spin-asymmetry parameter $l_{L\downarrow}/l_{L\uparrow} \sim 0.14$. At the same time, in Ni with Cr impurities $l_{L\downarrow}/l_{L\uparrow} \sim 1.5$. The wide range of the spin-asymmetries variations opens up a new way to optimize the magnetoresistive properties of magnetic nanocontacts. Before we proceed with the results, note here that strong dependence of the magnetoresistance on mean-free paths is a particular feature of nanocontacts, because their size in comparable with the conduction electron mean-free paths [6,7].

Figure 8 shows the case when one ferromagnet has essentially higher conduction electron density compared with the other. The absolute values of the MR effect are not so exciting, especially from the point of view of magnetic field sensor applications, however, MR can be not only positive, but also negative depending on combination of the spin-asymmetries of the contacting ferromagnets (see Fig. 8b, 8c and 8e) [6].

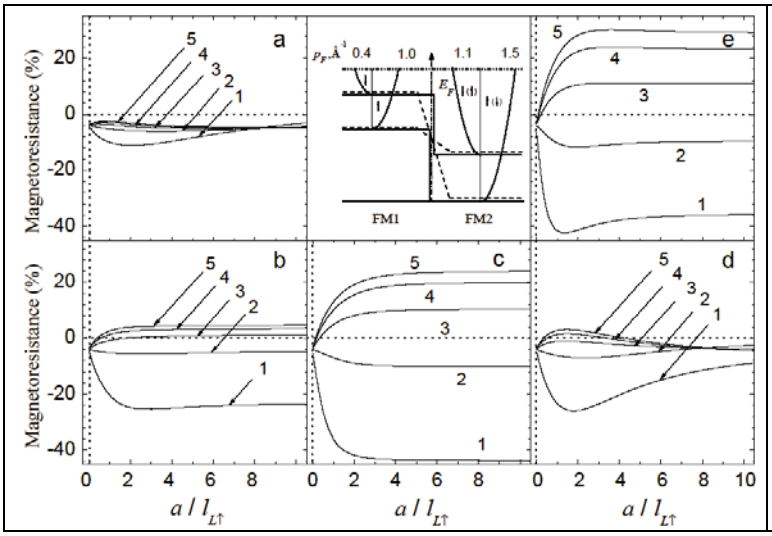

Fig. 8. The same as in Figure 7, but for the ferromagnetic heterocontact. The parameters of the ferromagnets are: $\delta_L = p^L_{F\downarrow}/p^L_{F\uparrow} = 0.4$, $\delta_R = p^R_{F\downarrow}/p^R_{F\uparrow} = 0.73$. The conduction-band matching diagram is given in the central window of the first row.

Figure 9 shows the case when one ferromagnet has a bit higher conduction electron density compared with the other. The absolute values of the MR effect ~130% are much higher in the ballistic limit ($a/l_{L\downarrow}$<<1) than in the previous case. Again, figures 9d and 9e show nonmonotonic behavior of MR as a function of the contact radius. The figures 9b, 9c and 9e suggest combinations of parameters, for which MR keeps high values with increasing the contact cross-section.

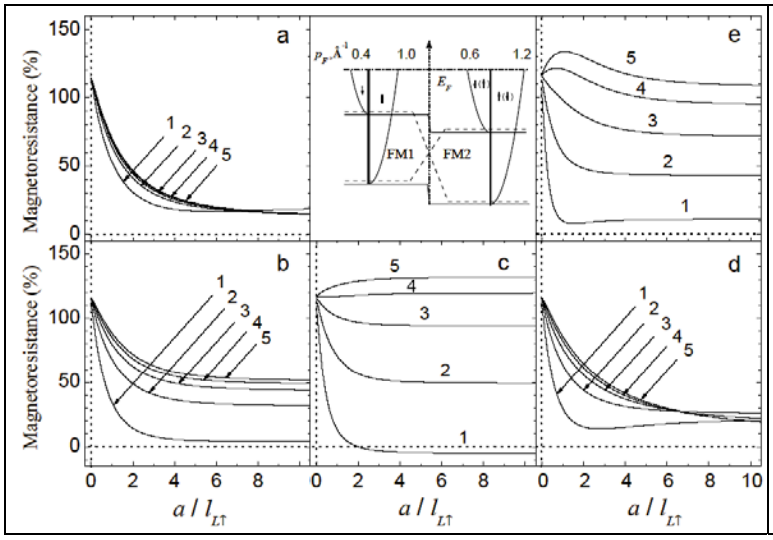

Fig. 9. The same as in Figure 7, but for the ferromagnetic heterocontact. The parameters of the ferromagnets are: $\delta_L = p^L_{F\downarrow}/p^L_{F\uparrow} = 0.4$, $\delta_R = p^R_{F\downarrow}/p^R_{F\uparrow} = 0.5$. The conduction-band matching diagram is given in the central window of the first row.

Figure 10 (a to d) shows the case of the contact when ferromagnets have similar conduction electron densities but different spin polarizations of the conduction band. Although MR magnitudes are moderate, Figs. 10b and 10c suggest a weak dependence of MR on the contact radius at certain combinations of the MFP spin asymmetries (see the figure caption). Thus, have shown for the first time that a material parameters combination can be found, for which the magnetoresistance keeps high magnitudes even in the diffusive regime of conductance on the scale of the nanocontact size. We refer this effect to a gradual change in conductance regime when increasing the contact size: from ballistic to one of the spin-channels and diffusive for the second one, to the both spin-channels of conduction becoming in the diffusive regime.

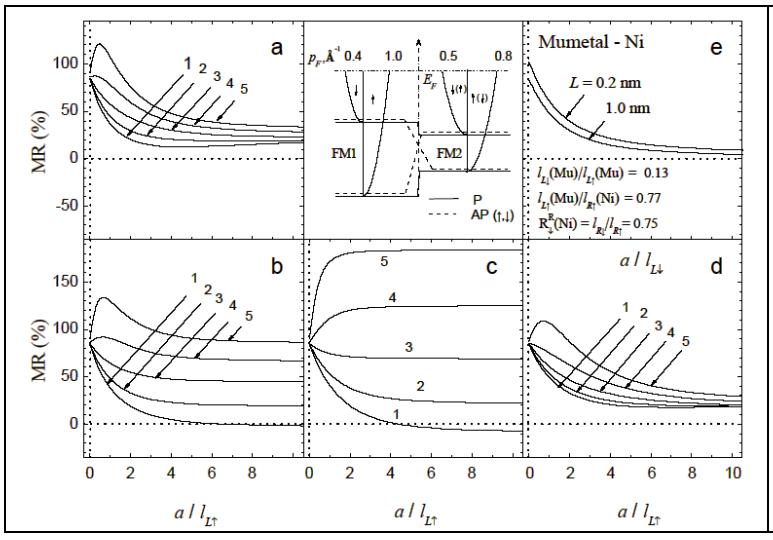

Fig. 10. The same as in Figure 7, but for the ferromagnetic heterocontact. The parameters of the ferromagnets are: $\delta_L = p^L_{F\downarrow}/p^L_{F\uparrow} = 0.4$, $\delta_R = p^R_{F\downarrow}/p^R_{F\uparrow} = 0.63$. The conduction-band matching diagram is given in the central window of the first row.

The **sub-task 6.2.1** was carried out in collaboration with Prof. N. Garcia. The

boundary resistance of interface between two contacting conductors has been extensively studied [8,9,21-24]. The spin-dependent boundary resistance has crucial contribution to the giant magnetoresistance effect. From analysis of the experimental data it was found that there is incredible discrepancy between experimentally estimated boundary resistance of a contact, and boundary resistance calculated from existing quasiclassical theories. In the result of extensive studies it was established that commonly accepted quasiclassic boundary condition, at which the boundary resistance of the interface between two metals is calculated as an integrated ballistic *single-conductance-channel* resistance, is **incorrect**. The original solution of the problem is proposed, which formulates the ballistic boundary resistance (or conductance) in terms of successive approximations to the correct, *multi-channel* resistance (or conductance) of interface (see Figure 11 below) [8,9].

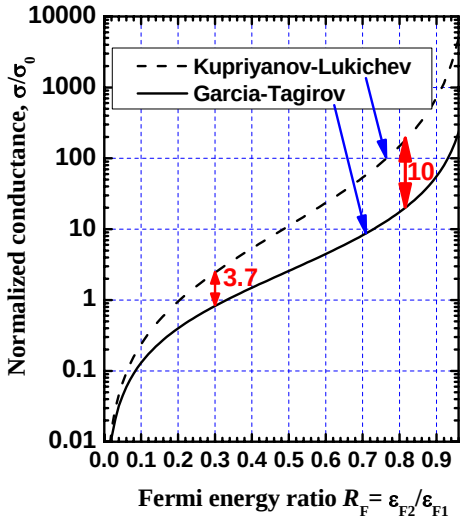

Fig. 11. Dependence of the interface conductance (inverse boundary resistance) on the Fermi energy ratio of contacting metals. Ordinate scale is logarithmic.

The novel formulation relaxes an order of magnitude discrepancy between theory and experiment (see the figure) when the experimental data are treated using the old boundary resistance theory with physical parameters of the materials in the contact. The theory deepens and extends our understanding of electric and spin transport through interfaces between two metals in a contact.

Sub-task 6.2.2. Another model of a heterocontact includes a nonmagnetic metal in a contact with a ferromagnetic metal. The model matches actual nanoconstriction samples fabricated by CCLRC/CRIST team. They consist of a trilayer: tantalum/permalloy/tantalum, and contact pads for connection to external current and potential terminals have been made of nonmagnetic metal. As we already established during the first year of the project implementation, the interface between two non-identical metals produce boundary resistance which may contribute the total resistance of the device. Within our new, quasiclassical multi-channel approach to derivation of the boundary conditions, we calculated the spin asymmetry and the absolute value of the boundary resistance [9,10,24]. Original formulas have been obtained for the first time for

these important physical quantities, and comparison with the existing experimental data has been made to validate quantitative correctness of the obtained expressions [9,10]. Figure 12, from *a* to *c*, shows results of calculations of the spin-asymmetry of the boundary resistance, absolute value of the boundary resistance, as well as results of estimations of the physical parameter for Co/Cu, Co/Ag and Co/Cr contacts, for which we have reliable experimental data.

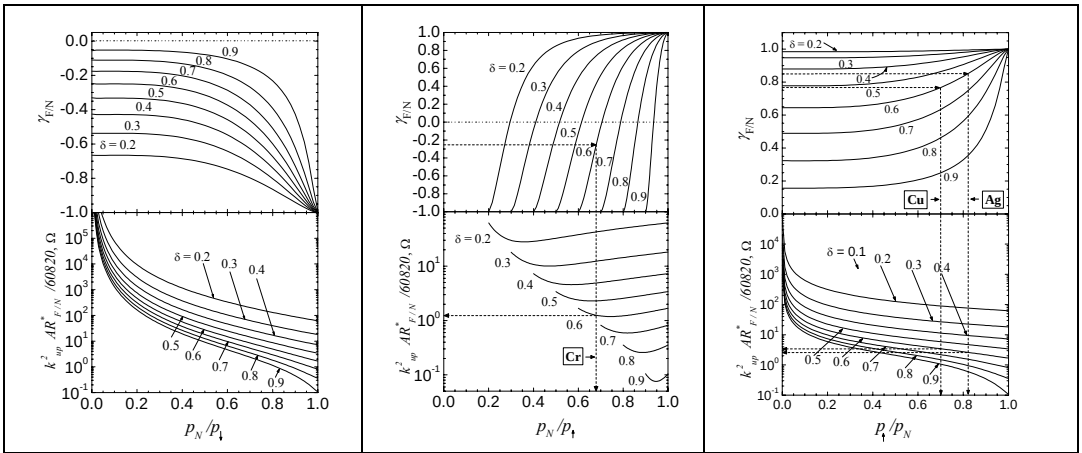

Fig. 12. Dependence of the spin-asymmetry, $\gamma_{F/N}$, and the absolute value of the boundary resistance, $R_{F/N}$, on the magnitude of the non-metallic metal Fermi momentum, p_N. Three cases correspond to a low conduction electron concentration metal (left graph, $p_\uparrow > p_\downarrow > p_N$), intermediate concentration metal (middle graph, $p_\uparrow > p_N > p_\downarrow$) and very high conduction electron concentration metal (right graph, $p_N > p_\uparrow > p_\downarrow$) (see in more details and examples in [9]).

Both the sign and magnitude of the spin asymmetry, and the absolute value of the boundary resistance have shown excellent agreement with the experiments. The optimization condition that the Fermi momentum of the non-magnetic metal has to be as close as possible to the majority/minority subband Fermi momenta of a ferromagnetic metal in a contact (which one depends on the magnitude of the non-magnetic spacer metal with respect to the ferromagnet's majority and minority Fermi momenta, as well as the spin-asymmetry of the bulk impurity scattering) has been derived from our calculations. Now, for the first time, we have a quantitative tool to estimate contribution of the ferromagnetic metal – non-magnetic metal interface resistance (which is parasitic one in our device contructions) into the total resistance of the nanocontacts studied in the project.

The **sub-task 6.2.3** accomplishes the study of tunnelling magnetoresistance in magnetic tunnelling nanocontacts. In the framework of the quasiclassical theory, that we developed for magnetic nanocontacts, we calculated tunnelling magnetoresistance of ferromagnetic nanocontacts [11,26]. The theory is most general to consider the physical parameters of contacting metals, and gives universal forms of equations were boundary conditions of the area of the contact include spin-dependent quantum-mechanical coefficient of transmission through the insulating layer. The ferromagnets can be either identical or different, the Fermi momenta of conduction electrons in the spin-subbands, as well as spin-dependent mean free paths $l_{L(R)}$ of the both ferromagnets can be arbitrary.

The tunnelling magnetoresistance (TMR) of nanocontacts was calculated in a wide range of parameters of contacting ferromagnetic metals, as well as of the insulating barrier. Figure 1 shows the bias voltage dependence of TMR for different thickness L of the insulating barrier (left), and for different spin-asymmetries $l_{L\uparrow}\backslash l_{L\downarrow}$ of the bulk mean free paths in the ferromagnetic electrodes (middle). The general conclusion is that TMR oscillations for high biases strongly depend on the thickness of the barrier, as well as there is sizeable influence of the mean free paths on TMR. The latter dependence is characteristic for nanocontacts, because cross-section size is comparable with the mean free paths. For the case of laterally infinite tunnelling contacts there is no dependence of TMR on the electron mean free paths.

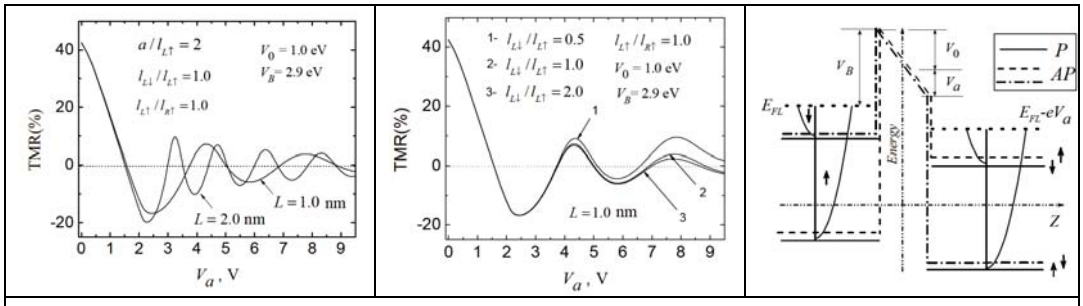

Fig. 13. Tunneling magnetoresistance of a ferromagnetic heterocontact. Left window – the dependence of TMR on the barrier thickness (indicated in the figure). Middle window – the dependence of TMR on the spin-asymmetry of mean-free paths in ferromagnetic electrodes. The material parameters are indicated in the figure. Right-hand-side window – the potential landscape in vicinity of the tunnelling nanocontact subject to the external bias voltage V_a. The conduction-band polarization parameter is $\delta_L = p^L_{F\downarrow}/p^L_{F\uparrow} = 0.73 = \delta_R$.

Figure 2 shows bias voltage dependence of TMR at different spin-polarizations of the conduction band, and the two heights of the insulating barrier corresponding to alumina (1.2 eV) and magnesium oxide (2.9 eV).

Our calculations show that the general tendency for TMR to decrease with increasing the bias voltage takes place for nanocontacts as well as for planar structures. At low enough voltages (1V and lower) the theory predicts high enough TMR values which can be interesting for applications. The particular feature of the tunnelling nanocontacts is that these high magnitudes of TMR have been obtained without special

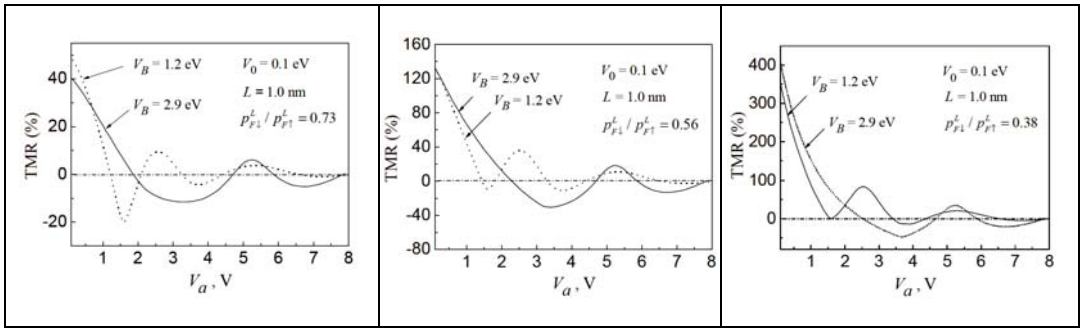

Fig. 14. Tunneling magnetoresistance of a ferromagnetic nanocontact – dependence on the bias voltage. Left window – drawn for the conduction band polarization $\delta = p_{F\downarrow}/p_{F\uparrow} = 0.73$, middle window – drawn for the conduction band polarization $\delta = p_{F\downarrow}/p_{F\uparrow} = 0.56$, and right window – drawn for the conduction band polarization $\delta = p_{F\downarrow}/p_{F\uparrow} = 0.38$. Other parameters are indicated in the figure.

requirements to the barrier crystalline structure as well as special matching of wave functions between the barrier and the ferromagnets. Thus, we suggest that the tunnelling nanocontacts may compete with the planar structures in obtaining the high TMR values.

Workpackage 8 (Optimization and further investigation)

The KSU group was charges by accomplishing Task 8.3 of the Woprkpackage 8, analysis of findings: "Then, a series of studies on the factors influencing the BMR can be carried out in the project, including the effect of different ferromagnetic materials, different nanocontact materials (magnetic, nonmagnetic and magnetic/semiconductor), domain wall profiles, and different degree of spin polarization, which will lead to a better understanding of the BMR effect and the discovery of new structures and new mechanisms for spin-dependent electronic transport in thin film nanocontacts."

The activity in the framework of the **Workpackage 8** was devoted to optimization of the magnetoresistive properties of magnetic heterocontacts using the additional degrees of freedom that the quasiclassical theory offers operating with arbitrary spin-polarizations of the conduction band of ferromagnetic electrodes and spin-dependent mean free paths.

Figure 15 suggests that maximal values of the spin-asymmetry of the surface scattering (modulus is equal to one) are achieved when the Fermi momentum of the nonmagnetic spacer is equal to one of the Fermi momenta of the ferromagnet's conduction spin-subband (upper panels in the graphs below). Then the GMR effect magnitude is maximal. It is a criterion for maximizing the GMR effect in Ferromagnet-Non-magnetic metal layered structures.

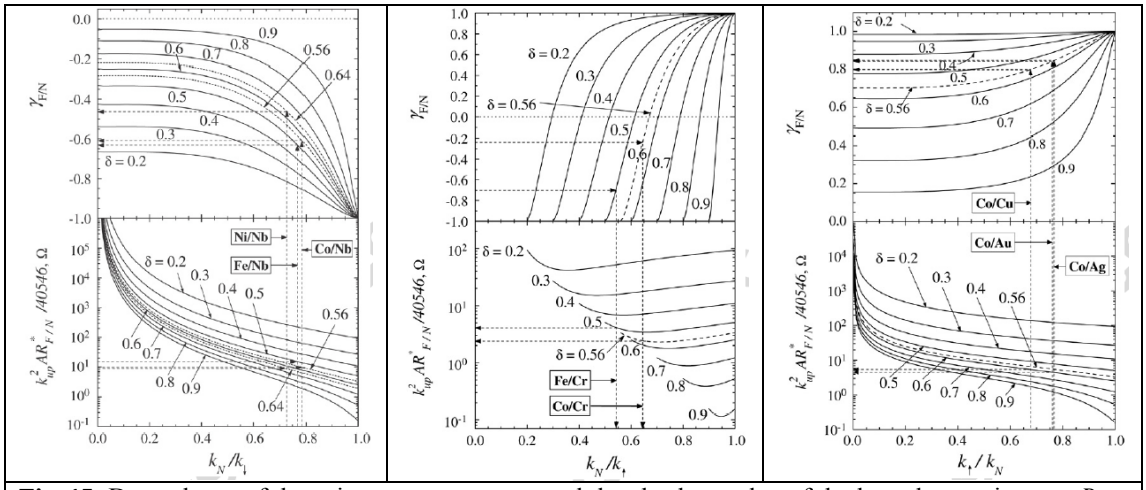

Fig. 15. Dependence of the spin-asymmetry, $\gamma_{F/N}$, and the absolute value of the boundary resistance, $R_{F/N}$, on the magnitude of the non-metallic metal Fermi momentum, p_N. Three cases correspond to a low

conduction electron concentration metal (left graph, $p_\uparrow > p_\downarrow > p_N$), intermediate concentration metal (middle graph, $p_\uparrow > p_N > p_\downarrow$) and very high conduction electron concentration metal (right graph, $p_N > p_\uparrow > p_\downarrow$) (see in more details and examples in [9]).

Figure 16 (a to d) shows a case which corresponds to Mumetal-Nickel heterocontacts. Mumetal ($Ni_{77}Fe_{14}Cu_5Mo_4$) is close to Permalloy ($Ni_{80}Fe_{20}$) in its composition, hence, it has very short mean free path in the spin-down conduction channel (in permalloy, $l_{L\downarrow} \approx 6$Å, whereas $l_{L\uparrow} \approx 46$Å, so that the spin-asymmetry parameter $l_{L\downarrow}/l_{L\uparrow} \sim 0.13$). The larger spin-dependent Fermi momentum in Ni has been assigned to the spin-down subband which has higher density of states according to the spin-polarized density-of-state calculations (see, for example, J.M.D. Coey, in: Spin Electronics, Springer Lecture Notes in Physics, v. 569 edited by M. Ziese and M.J. Thornton, Springer-Verlag 2001, p. 279). The results of calculations are given in Fig. 16e. For ballistic regime of conductance ($a/l_{L\downarrow} \to 0$) MR is close to 100% (L = 0.5 nm) which agrees satisfactorily with the experimental values of MR = 78-132%, Fig. 2 in Y.-W. Zhao, M. Muñoz, G. Tatara, N. García, J. Magn. Magn. Mater. 223, 169 (2001), at low conductance for the P-alignment of magnetizations.

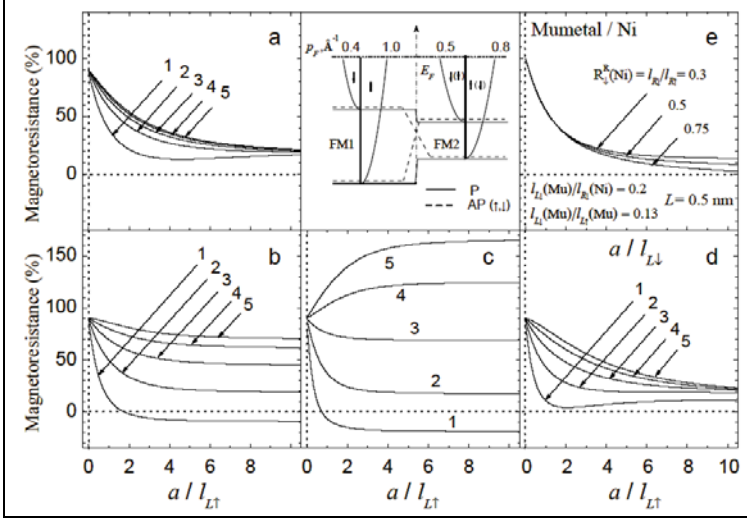

Fig. 16. Magnetoresistance of a nanocontact appropriate to a heterocontact Mumetal-Nickel. The parameters of the ferromagnets are: $\delta_L = p^L_{F\downarrow}/p^L_{F\uparrow} = 0.4$, $\delta_R = p^R_{F\downarrow}/p^R_{F\uparrow} = 0.63$. The conduction-band matching diagram is given in the central window of the first row. The plot (e) shows dependence of MR on a for the choice of parameters appropriate to the heterocontact Mumetal-Ni.

Our calculation suggests the choice of parameters (corresponds to Fig. 16c), from which magnetoresistance does not drop with increasing the nanocontact cross-section. This finding relaxes the requirement of nanometric contact size to obtain high magnitudes of magnetoresistance in magnetic nanocontacts.

Another portion of activity in the framework of the **Workpackage 8** was devoted to calculations of the electric resistance, magnetic domain structures and magnetoresistance of the actual nanostructures fabricated and characterized by the CCLRC/CRIST/CSIC team. The constriction-type nanostructure domain configurations, electric resistance and magnetoresistance calculations are in big progress to be used for understanding and optimization of the magnetoresistive properties. The distribution of the electric resistance along the nanocontacts is calculated (see an example below, Figure 17).

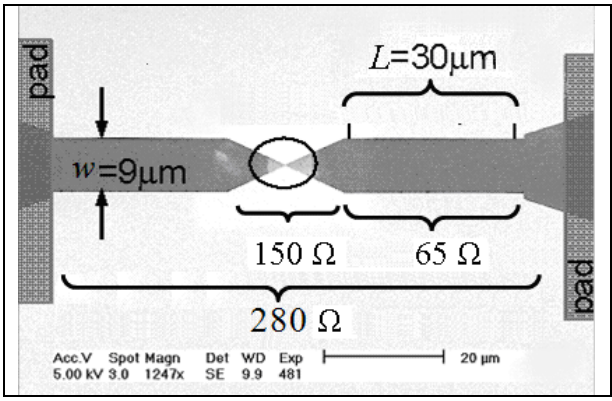

Fig. 17. The SEM image of the nanocontacts with calculated resistances of the fragments. The exact geometry of the nanocontacts as well as trilayer film structure, Ta(2.5nm)/Py(7nm)/Ta(2.5nm), and experimental values of the resistivities of the metals have been accounted for.

The anisotropic magnetoresistance of the samples has been calculated. The magnitude of the effect (about 0.5 Ohm) is not sufficient to explain 5-8 Ohm of resistance change in magnetic field observed in the experiment. We have analyzed also the Levi-Zhang mechanism of the impurity scattering enhancement in the domain wall (Levy-Zhang, Physical Review Letters 79, 5110 (1997)). The conclusion is that the Levy-Zhang mechanism can explain the magnitude of magnetoresistance observed in the experiment. The magnetoresistance figures may exceed few tens percents depending on the domain wall width. The micromagnetic calculations of the magnetic domain configurations and magnetic hysteresis are in big progress. They will be compared with experimental data on magnetic configurations and domain wall structures when available from the partners experiments.

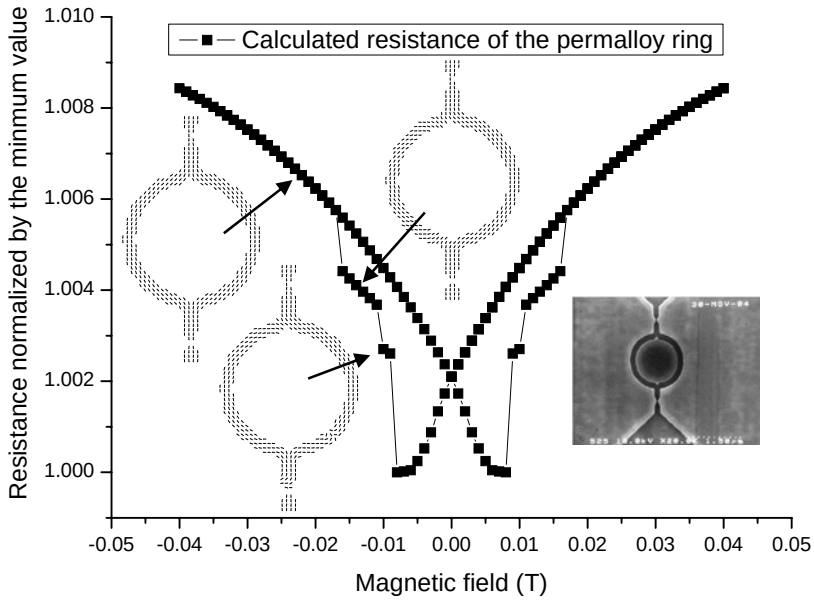

Fig. 18. Calculated magnetic configurations of the ring and electric resistance versus magnetic field.

The magnetic moment configurations, magnetic hysteresis and dependence of the

electric resistance on magnetic field have been calculated for mesoscopic ferromagnetic rings to understand their magnetoresistive properties (Fig. 18). The calculations can be adjusted to the geometry and the magnetic field direction with respect to the symmetry axis of the ring.

Section 2- Present state-of-the art of BMR research in the world

The theory for ballistic magneto-resistance was first proposed by Gerrit Bauer, (PRB 1998), in which he predicted a BMR of 230% obtainable in the ballistic transport regime. In 1999, Professor Nicolas Garcia (the coordinator of this project for the first 24 months) published the first ever experimental result of BMR of 200% obtained from Ni wire nanocontacts (PRL 1999). Two years later, J. Coey, et al (PRL 2001), published the experimental BMR of 500% obtained in half metallic contacts. Harsh Chopra et al also published their experimental results (PRB 2002) with 3000% BMR in Ni nanocontacts. At that time, there have been huge publicity and expectations about the ballistic magnetoresistance phenomenon. The present BMR project was proposed and awarded under such a background.

At the start of the project, there have been more publications on BMR, in particular Chopra et al have published their further work with BMR exceeds 100,000%. On the other hand, some reputable research laboratories in the world, such as NIST, Seagate Research and Cornell University have failed to reproduce the published experimental results even with the help of the authors. This has put the published work into question. For this reason, the 2004 joint MMM-Intermag conference had a special session - Symposium on the Controversy over Ballistic Magnetoresistance, in which the NIST group made their invited presentation "artifacts in ballistic magneto-resistance measurements". It is now widely believed that the very high BMR obtained in the published work originated from the effect of magnetostatic force interaction in the contact formed by the two wires. However, it is still not possible to conclude whether BMR exists. There are only a few groups in the world currently working on the topic: Cornell University, Toshiba Corporation and Tohoku University, but with very limited publications. So far, no convincing evidences have been reported regarding the existence of BMR in thin film nanocontacts.

Section 3 – Conclusions

Significant progress has been made the nanofabrication techniques by ebeam, nanoimprinting and FIB. Most of these techniques have been employed for the fabrication of CIP and CPP nanoconstrictions. However, some of them have not been successfully used for such a purpose due to technical difficulties in achieving the mix and match between optical lithography and the advanced nanofabrication techniques.

It has been found in this project that there have been several challenging issues for the realization of the spin dependent electron transport in thin film nanoconstrictions. The

nanofabrication for the sub-20 nm constriction sizes is a very challenging task on its own right. However, there are other equally important issues, such as the fine control of the magnetic anisotropy of the films, the design and control of domain structures near the constrictions, the physical quality of the constrictions and films and the protection of the constrictions from oxidation/contamination/ESD damage after their fabrication and during the magnet-transport measurement.

Following the special symposium of the 2004 joint MMM-Intermag conference on "the Controversy over Ballistic Magnetoresistance", it has been widely accepted that the published BMR results originated from the artifacts in the experimental measurement of the labs concerned. Although there have been continued efforts worldwide in the search on real BMR in thin film nanocontacts, no convincing experimental evidence has been published to date for the existence of BMR. The signature MR for single domain wall constriction observed in this project is the first of its kind which clearly demonstrate the spin-dependent transport of electrons through a single domain wall in these nanocontacts.

Our results have shown that the signature MR peaks at constriction sizes of 20 nm and decreases as the constriction sizes reduces. This is in contradiction to the BMR theory which predicted that ballistic magnetoresistance may be obtained in the ballistic transport regime where constriction size is smaller than the mean-free path of the conduction electrons, typically around 5 nm for NiF films. However, the reduction of MR in our experiment could be caused by a number of reasons, such as the ion radiation damage to the magnetic materials in the constrictions, or the change of the aspect ratio of the constriction sizes, both of which may prevent the formation of a single domain wall in the constriction and hence hinders the spin dependent ballistic transport in these very small constrictions. More investigations are required in order to understand the transport behaviors of the nanoconstrictions below 20 nm sizes.

Section 4 – Plan for using and disseminating the knowledge

The spin valve-like MR obtained from nanoconstrictions with single domain walls by in-situ FIB milling and MR Measuremenet is believed to be the most significant results obtained by the consortium along the lines of searching for BMR. We are in the process of writing a paper for publication in PRL.

Research grant applications in further exploring the above findings and in the experimental realisation of the two patents in spin Hall effect are being considered by the consortium.